AUTOPHAGY REPORTS
2024, VOL. 3, NO. 1, 2379193
https://doi.org/10.1080/27694127.2024.2379193

Taylor & Francis
Taylor & Francis Group

Altered lipid homeostasis and autophagy precipitate diffuse alveolar hemorrhage in murine lupus

Shuhong Han[a], Haoyang Zhuang[a], Yanpeng Diao[b], Mark Segal[b], Tanzia Islam Tithi[c], Weizhou Zhang[c] and Westley H. Reeves[a,c]

[a]Division of Rheumatology, Allergy, & Clinical Immunology; [b]Division of Nephrology, Hypertension, and Renal Transplantation; [c]Department of Pathology, Immunology, and Laboratory Medicine, University of Florida College of Medicine, Gainesville, FL 32610

ABSTRACT

Abnormal autophagy regulation is implicated in lupus and other autoimmune diseases. We investigated autophagy in the murine pristane-induced lupus model. Pristane causes monocyte/macrophage-mediated endoplasmic reticulum (ER) stress in lung endothelial cells and diffuse alveolar hemorrhage (DAH) indistinguishable from DAH in lupus patients. Enlarged macrophages with abundant lipid droplets containing neutral lipid and exhibiting increased autophagosome staining were observed in the lung and peritoneal macrophages after pristane treatment. Cellular overload of neutral lipid can lead to selective autophagy (lipophagy) of lipid droplets and transport to lysosomes. The autophagy inducer rapamycin decreased neutral lipid staining but aggravated DAH, while an autophagy inhibitor (3-methyladenine) blocked the onset of DAH. Pristane-induced autophagy in macrophages was confirmed by acridine orange assay and LC3 western blot. Pristane also enlarged lysosomal volume and enhanced cathepsin S, D, and K expression while decreasing lysosomal acid lipase activity. If the capacity to degrade neutral lipid into free cholesterol and fatty acids is overwhelmed, lysosomes enlarge and can release cathepsins into the cytoplasm promoting cell death. Increasing lysosomal cholesterol content by blocking the Niemann-Pick C disease protein NPC1 protects against lysosome-dependent cell death. Treatment with NPC1 inhibitors U18666A or cepharanthine, which stabilize lysosomes, normalized lysosomal volume, reversed ER stress, and prevented DAH in pristane-treated mice. We conclude that pristane disrupts lipid homeostasis, promoting autophagy, lysosomal dysfunction, ER stress, and cell death leading to DAH. NPC1 inhibition reverses these abnormalities, preventing DAH. The findings shed light on the role of autophagy and lysosomal dysfunction in the pathogenesis of lupus

Abbreviations: 25HC, 25-hydroxycholesterol; 3MA, 3-methyladenine; ACAT, acyl-coenzyme A: cholesterol acetyltransferase; AO, acridine orange; B6, C57BL/6 mice; BODIPY, 4,4-difluoro-1,3,5,7,8-pentamethyl-4-bora-3a,4a-diaza-

CONTACT Shuhong Han shuhong.han@medicine.ufl.edu Division of Rheumatology & Clinical Immunology, University of Florida, PO Box 100221, Gainesville, FL

Supplemental data for this article can be accessed online at https://doi.org/10.1080/27694127.2024.2379193.

s-indacene; Ch25h, cholesterol 25-hydroxylase; DAH, diffuse alveolar hemorrhage; ER, endoplasmic reticulum; IFN, interferon; LAL, lysosomal acid lipase; LAMP-1, lysosomal-associated membrane protein 1; LDCD, lysosome-dependent cell death; LDL, low density lipoprotein; LMP, lysosomal membrane permeabilization; LPS, lipopolysaccharide; LXR, liver X receptor; Mφ, macrophage; MFI, mean fluorescence intensity; MO, mineral oil; mTORC, mechanistic target of rapamycin complex 1; NPC1, Niemann-Pick C disease protein 1; PI3K, phosphoinositide 3-kinase; PECs, peritoneal exudate cells; qPCR, quantitative real-time PCR; SLE, systemic lupus erythematosus; TFEB, transcription factor EB; TUNEL, terminal deoxynucleotidyl transferase dUTP nick end labeling; UPR, unfolded protein response; PECs, peritoneal exudate cells.

ARTICLE HISTORY Received: 11 Aug 2023; Revised: 01 Jul 2024; Accepted: 05 Jul 2024

KEYWORDS Cholesterol; Endoplasmic reticulum stress; Lipid droplets; Lysosomes; Macrophages; Lung; Niemann-Pick C disease; Pristane; Rapamycin; Systemic lupus erythematosus

Introduction

Systemic lupus erythematosus (SLE) is a systemic autoimmune disease with protean clinical presentations including antinuclear antibodies, renal, skin, nervous system, hematological, and pulmonary manifestations.[1] The chronic inflammatory response to intraperitoneal injection of the hydrocarbon oil pristane (2,6,10,14-tetramethylpentadecane) in non-autoimmune-prone mice causes a type I interferon-dependent lupus syndrome closely mimicking human SLE.[2] Other hydrocarbon oils, such as mineral oil (MO) cause chronic peritoneal inflammation, but not lupus. Mice with pristane-induced lupus develop lupus autoantibodies, glomerulonephritis, arthritis, and hematological abnormalities typical of human SLE. Pristane treatment also alters the function of macrophages (Mφ) and monocytes, which play an important role in disease pathogenesis.[3,4]

Pristane-induced lupus in C57/BL6 (B6) mice is complicated by severe diffuse alveolar hemorrhage (DAH) with pulmonary vasculitis closely resembling DAH in lupus patients.[2] Administration of liver X receptor (LXR) agonists, such as T0901317, prevents this complication.[5] While the protective effect of T0901317 may be due to its influence on Mφ polarization, LXR activation also facilitates reverse transport of free cholesterol out of the cell via the LXR-regulated ATP-binding cassette subfamily A member 1 (Abca1).[6,7] In pristane-treated mice with DAH, an unfolded protein response (UPR) develops in lung tissue, leading to endoplasmic reticulum (ER) stress of endothelial cells and apoptotic cell death.[8] Elevated levels of free cholesterol and long-chain saturated fatty acids can induce ER stress and cell death, termed "lipotoxicity".[9,10]

The transport of lipids between cellular compartments relies on a complex network of pathways centered on lysosomes, which have emerged as master regulators of lipid metabolism.[11] Apart from *de novo* synthesis, lipids can

enter the cell through cell surface receptors, such as low-density lipoprotein (LDL) receptors[12] or receptors for dead cells.[13] Lysosomal acid lipase (LAL) degrades the lipids, generating fatty acids and free cholesterol, which can be recycled or transported out of the cell. Conversely, cholesterol can be re-esterified and stored as lipid droplets.[14]

Disruption of lysosomal lipid homeostasis is toxic to cells resulting in lysosomal membrane permeabilization (LMP) and the release of lysosomal proteases into the cytoplasm, which can cause cell death. Lysosome-dependent cell death (LDCD) is a form of regulated necrotic cell death that follows LMP.[15] Accumulation of cholesterol in the lysosomes enhances lysosomal stability and prevents LMP.[16] We investigated the potential involvement of lipotoxicity and lysosomal dysfunction in pristane-induced DAH.

Results

Monocyte/Mφ depletion prevents pristane-induced DAH.[3] Circulating proinflammatory non-classical monocytes with the unusual phenotype $CD11b^{+}Ly6C^{-}CD138^{+}$ are seen in pristane-treated B6 mice with DAH, but not in MO-treated B6 mice or pristane-treated BALB/c mice, which do not develop DAH.[4,17] However, their role in DAH is unclear.

Pristane causes lipid accumulation in monocytes and Mϕ

Consistent with prior observations,[3,8] lipid-laden Mϕ were detected histologically in the lungs (Figure 1A, top) and PECs (not shown) of pristane-treated mice. Lung Mϕ from untreated mice were smaller and did not contain prominent vacuoles as seen in pristane-treated mice. We examined whether vacuoles in monocytes/Mϕ contained neutral lipid by flow cytometry. As shown in Figure 1B, both $CD138^{+}$ blood monocytes and $CD138^{+}$ peritoneal Mϕ from pristane-treated mice stained strongly with Nile red. In pristane-treated mice, staining was more intense in $CD138^{+}$ blood monocytes than in peritoneal $CD138^{+}$ or $Ly6C^{hi}$ Mϕ or circulating neutrophils (Figure 1B-C). Nile red staining was higher in peritoneal $CD138^{+}$ Mϕ, $Ly6C^{hi}$ Mϕ, and neutrophils from pristane-treated mice vs. MO-treated controls and was stronger in $CD138^{+}$ Mϕ vs. $Ly6C^{hi}$ (classical) Mϕ or neutrophils (Figure 1D). A similar pattern was seen in PECs stained with BODIPY 493/503, another lipophilic dye that stains neutral lipids (Figure 1E). Nile red and BODIPY 493/503 staining was strongest in $CD138^{+}$ Mϕ.

Lipid droplets are organelles that store neutral lipids.[18] *Plin2*, encoding the lipid droplet-specific protein perilipin-2 (adipophilin), is the most highly overexpressed gene in Mϕ exposed to oxidized LDL (Ox-LDL).[19] It impairs lipid mobilization in foamy Mϕ, promoting atherosclerosis[20] and is upregulated in cerebral ischemia/reperfusion resulting in NLRP3-mediated inflammation.[21]

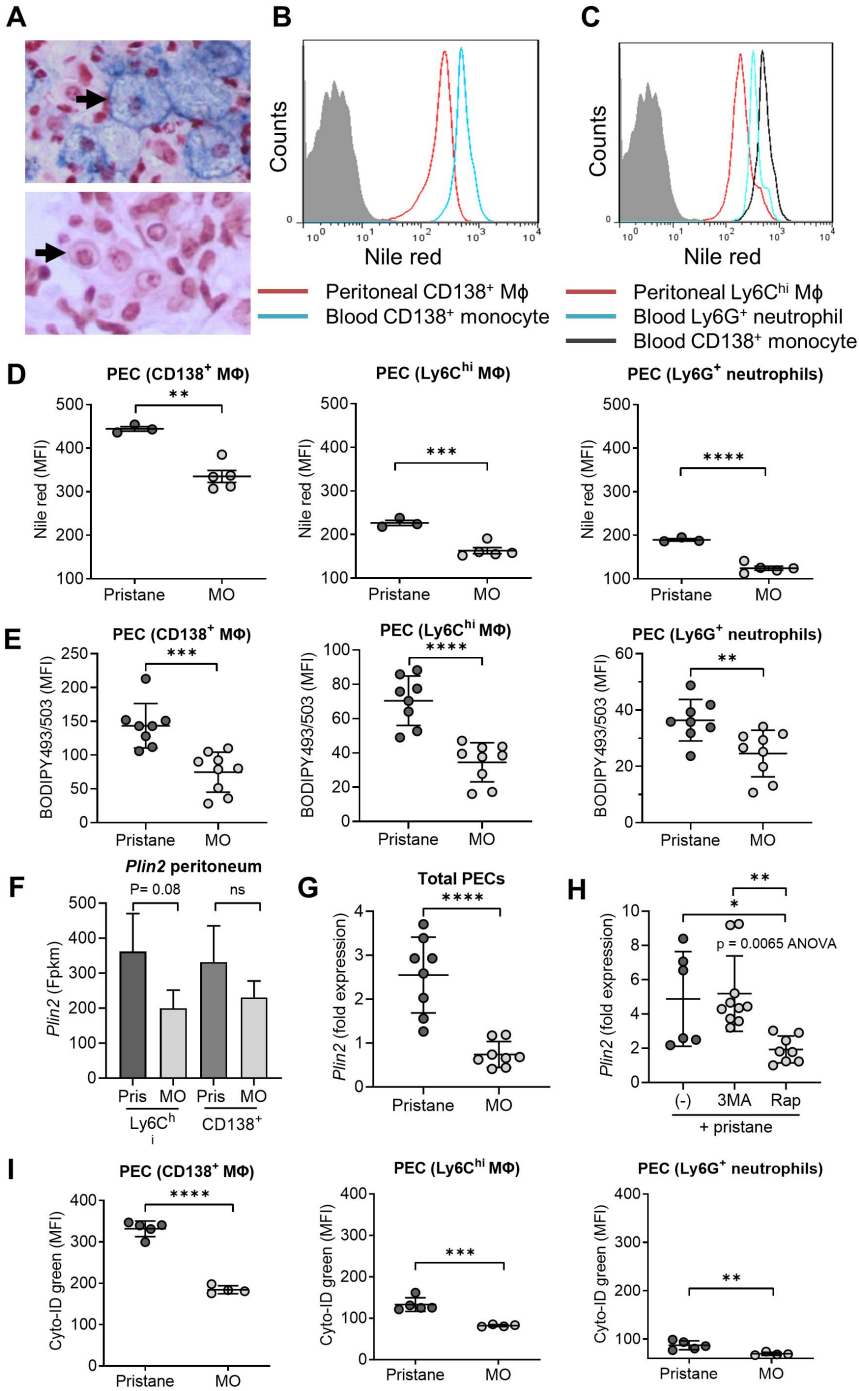

Figure 1. *Neutral lipid accumulation and autophagosome formation in pristane-treated mice.* B6 mice were treated with pristane or mineral oil (MO) and 14-d later were

Plin2 deficiency protects against atherosclerosis and non-alcoholic steatohepatitis by reducing inflammation.[22] RNA-Seq analysis suggested that *Plin2* expression was higher in pristane- vs. MO- treated Ly6C^{hi} and CD138^{+} Mϕ (Figure 1F). Upregulation of *Plin2* was confirmed by qPCR in PECs from pristane- vs. MO- treated mice (Figure 1G), suggesting that pristane treatment increased lipid droplet formation.

Selective autophagy of lipid droplets (lipophagy) transports neutral lipids to lysosomes, where they are degraded by LAL.[23–25] Excessive lipid accumulation or metabolic stress upregulates lipophagy, whereas inhibition of autophagy promotes lipid droplet formation.[25] Inside the lysosome, perilipin-2 regulates access of LAL to the lipid droplet core, impairing lipid droplet degradation.[14,26] When mice were treated with pristane plus an autophagy inhibitor (3-methyladenine, 3MA), *Plin2* expression in PECs was unaffected (Figure 1H). In contrast rapamycin, an mTOR inhibitor that induces autophagy, decreased *Plin2* (Figure 1H), suggesting that it might enhance the degradation of neutral lipid by LAL.

In comparison with controls, pristane treatment greatly increased autophagosome volume as demonstrated by cyto-ID green staining (Figure 1I). High Cyto-ID green staining was associated with high neutral lipid staining, as both were highest in peritoneal CD138^{+} Mϕ, intermediate in Ly6C^{+} Mϕ, and lower (but still enhanced by pristane) in Ly6G^{+} neutrophils (Figure 1I). These studies indicate that exposure to the DAH-inducing oil pristane, but not a

examined for lipid accumulation. (**A**), H&E staining of lung tissue from a pristane-treated mouse (top) showing enlarged macrophages (Mϕ) with numerous cytoplasmic vacuoles. Lung Mϕ from an untreated control (bottom) were smaller with less prominent vacuoles. (**B**), Flow cytometry of Nile red-stained peritoneal Mϕ and circulating monocytes from mice treated 14-d earlier with pristane. *Red*, peritoneal CD11b^{+}CD138^{+} Mϕ; *Blue*, circulating CD11b^{+}CD138^{+} monocytes. (**C**), Flow cytometry of Nile red-stained Mϕ and circulating monocytes from mice treated 14-d earlier with pristane. *Red*, peritoneal CD11b^{+}Ly6C^{hi}CD138^{-} Mϕ; *Blue*, circulating CD11b^{+}Ly6G^{+} neutrophils; *Gray*, circulating CD11b^{+}Ly6C^{-}CD138^{+} monocytes. (**D**), Nile red staining of total PECs from pristane and MO treated mice (MFI, mean fluorescence intensity). *Left*, CD11b^{+}Ly6C^{-}CD138^{+} Mϕ; *middle*, CD11b^{+}Ly6C^{hi}CD138^{-} Mϕ; *right*, CD11b^{+}Ly6G^{+} neutrophils. (**E**), BODIPY 493/503 staining of total PECs from pristane and MO treated mice. *Left*, CD11b^{+}Ly6C^{-}CD138^{+} Mϕ; *middle*, CD11b^{+}Ly6C^{hi}CD138^{-} Mϕ; *right*, CD11b^{+}Ly6G^{+} neutrophils. (**F**), RNA-Seq showing relative expression of *Plin2* mRNA in peritoneal CD11b^{+}Ly6C^{hi}CD138^{-} Mϕ and CD11b^{+}Ly6C^{hi}CD138^{-} Mϕ from pristane vs. MO treated mice (Fpkm, fragment per kilobase million). (**G**), *Plin2* expression in total PECs from pristane- vs. MO- treated mice. (**H**), *Plin2* expression in pristane treated mice receiving 3-methyladenine (3MA), rapamycin (Rap), or pristane alone (-). (**I**), Cyto-ID green staining of total PECs from pristane and MO treated mice. *Left*, CD11b^{+}Ly6C^{-}CD138^{+} Mϕ; *middle*, CD11b^{+}Ly6C^{hi}CD138^{-} Mϕ; *right*, CD11b^{+}Ly6G^{+} neutrophils. **, $P < 0.01$; ***, $P < 0.001$, ****, $P < 0.0001$, ns, not significant (Student t-test).

control oil (MO), altered lipid homeostasis and that neutral lipid accumulation was accompanied by evidence of increased autophagy.

The induction of autophagy by pristane was confirmed by acridine orange (AO) staining and the conversion of LC3-I to LC3-II (Figure 2). In comparison with MO treatment, pristane treatment greatly augmented the AO red/green fluorescence ratio in $CD138^+$ and $CD138^-$ peritoneal Mϕ at d-14 (Figure 2A). By this assay, autophagy was not significantly higher in $Ly6G^+$ neutrophils from pristane vs. MO treated mice.

We compared the effect of rapamycin, a known autophagy inducer, with that of pristane in murine Mϕ (RAW264.7 cell line) (Figure 2B-C). As expected, rapamycin dose-dependently increased the AO red/green fluorescence, consistent with the induction of autophagy (Figure 2B, left). 3MA inhibited rapamycin-induced autophagy in a dose-dependent manner (Figure 2B, right). Similarly, incubation of RAW264.7 cells with pristane dose-dependently increased AO red/green fluorescence (Figure 2C, left). Pristane-induced autophagy in RAW264.7 cells also was inhibited dose-dependently by 3MA (Figure 2C, right).

We also cultured RAW264.7 cells with/without pristane followed by western blotting for LC3-I (16-18 kDa) and its lipidated form LC3-II (14-16 kDa), which migrates ahead of LC3-I due to its high hydrophobicity (Figure 2E). Incubation for 24-h with pristane substantially increased the LC3-II protein level in RAW264.7 cells vs. the level in RAW264.7 cells cultured without pristane. After culture with rapamycin (50 ng/mL) for 24-h, only a weak LC3-II signal was seen, most likely due to the kinetics of rapamycin induction of autophagy, which at doses ≥ 10 nM induces a rapid increase of LC3-II peaking at 30 min and then declining.[27]

Altered lipid homeostasis in pristane-induced DAH

We next explored the effects of rapamycin and 3MA on pristane-induced neutral lipid accumulation and lung hemorrhage. BODIPY 493/503 staining of lipid droplets in peritoneal $CD138^+$ Mϕ, $Ly6C^{hi}$ Mϕ, and neutrophils from pristane-treated mice was unaffected by 3MA (Figure 3A). In contrast, rapamycin decreased BODIPY staining in all three subsets (Figure 3A), suggesting that the accumulation of lipid droplets induced by pristane resolved when autophagy was enhanced.

Along with normalizing cytoplasmic neutral lipid accumulation, rapamycin treatment increased the frequency and severity of DAH in pristane-treated mice (Figure 3B). We also tested dactolisib, a dual PI3K-mTOR inhibitor, in 5 mice. Two mice died from DAH before day-14 and all three surviving mice had severe DAH. Despite the small number there was a trend toward worsening of DAH in this group ($P = 0.09$). Conversely, inhibition of autophagy with 3MA significantly reduced the frequency of DAH (Figure 3B). Together, the data

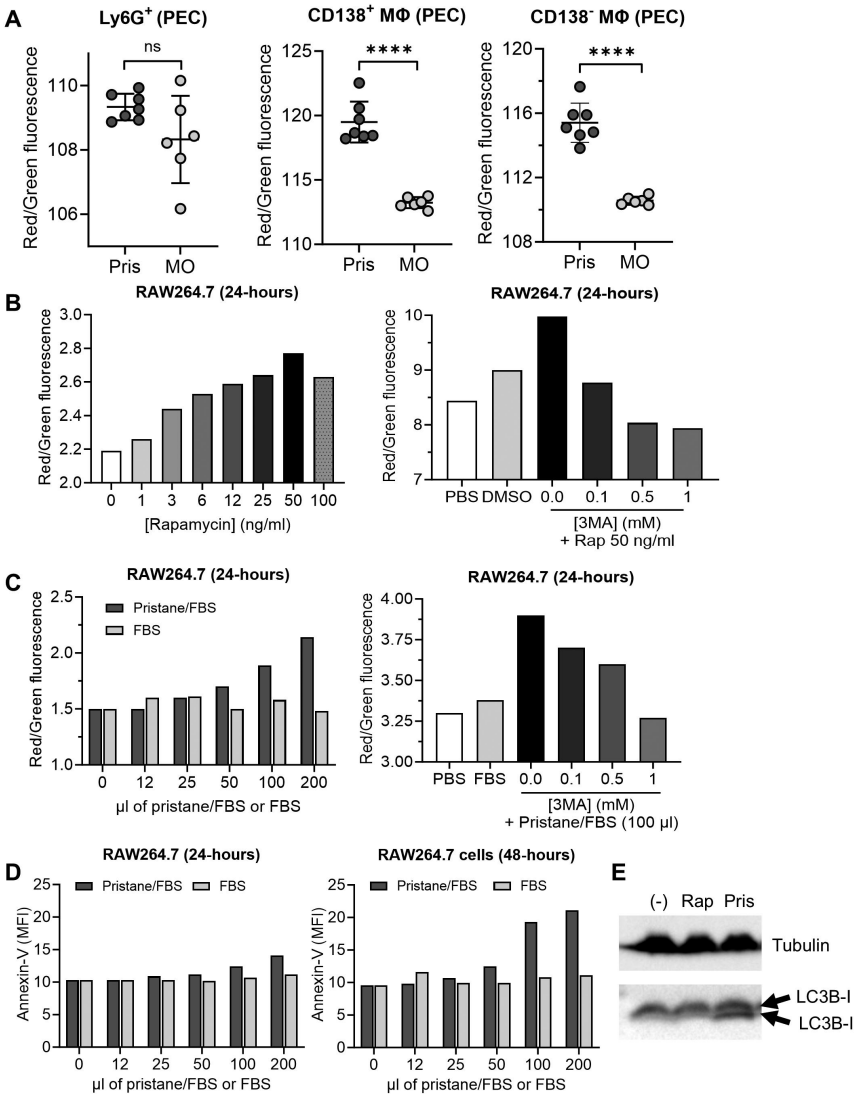

Figure 2. *Effects of pristane, rapamycin, and 3-methyladenine (3MA) on autophagy*. (**A**), B6 mice were injected i.p. with pristane (Pris) or mineral oil (MO) and 14-d later, autophagy was analyzed by acridine orange (AO) staining [red (Percp cy5.5 channel)/green (fluorescein isothiocyanate channel) fluorescence in flow cytometry] in Ly6G^{+} neutrophils, CD138^{+} Mϕ, and CD138^{-} Mϕ from peritoneal exudate cells (PEC). ****, $P < 0.0001$, Student t-test. ns, not significant). (**B**), *Left*, RAW264.7 Mϕ were incubated for 24-h in culture medium containing rapamycin (0-100 ng/mL) and AO staining (red/green ratio) was determined by flow cytometry. *Right*, RAW264.7 cells were cultured with rapamycin 50 ng/mL or carrier (DMSO) in the presence of 3MA (0, 0.1, 0.5, or 1.0 mM). AO staining (red/green ratio) was determined at 24-h by flow cytometry. Data are representative of two independent experiments. (**C**), *Left*, RAW264.7 Mϕ were incubated 24-h in culture medium containing 0-200 µL of fetal bovine serum (FBS) saturated with pristane (FBS/

suggest that increasing autophagy exacerbates DAH while inhibiting autophagy prevents it.

Lipophagy delivers lipid droplets to the lysosomes, where the neutral lipid is cleaved by LAL, yielding free cholesterol and fatty acids. We hypothesized that cleavage of cholesterol ester might explain why BODIPY 493/503 staining was lower in PECs from mice treated with pristane + rapamycin than in PECs from mice receiving pristane alone (Figure 3A). Lipophagy should generate an increased load of lysosomal free cholesterol, which is transported into the cytoplasm by the Niemann-Pick C disease proteins NPC1 and NPC2.[28,29] We investigated the role of lysosomal cholesterol transport in pristane-induced DAH using U18666A and cepharanthine, which are NPC1 inhibitors that mimic Niemann-Pick C disease.

U18666A treatment increases lysosomal cholesterol content by preventing its transport to the cytoplasm, and protects cells from lipotoxicity by stabilizing lysosomal membranes.[30] U18666A treatment potently inhibited pristane-induced DAH (Figure 3C). Treatment with cepharanthine, which also inhibits endolysosomal trafficking of free cholesterol by binding NPC1,[31] prevented DAH as effectively as U18666A (Figure 3C). As reported previously,[5] pristane-induced DAH was blocked by treatment with T0901317, a synthetic liver X receptor (LXR) agonist (Figure 3C). Although LXR activation re-polarizes Mϕ from a proinflammatory M1-like phenotype to an M2-like phenotype, it also enhances the expression of ATP-binding cassette transporter A1 (*Abca1*), which mediates reverse cholesterol transport across the plasma membrane, lowering cytoplasmic free cholesterol.[6,7]

Along with reverse cholesterol transport, cytoplasmic free cholesterol levels are reduced by esterification catalyzed by acyl-coenzyme A: cholesterol acetyltransferase (ACAT).[32] ACAT inhibitors impair cholesterol esterification, increasing free cholesterol in the ER membrane.[32] When the ACAT inhibitor avasimibe was given along with pristane, DAH was exacerbated (Figure 3D). Thus, pristane-induced DAH could be prevented by activating Abca1-

pristane), or with FBS alone. *Right*, RAW264.7 cells were cultured in DMEM medium for 24-h with FBS/pristane (100 µL) or with FBS alone in the presence/absence of 3MA (0, 0.1, 0.5, or 1.0 mM). Data are representative of two independent experiments. (**D**), RAW264.7 Mϕ were incubated 24-h in DMEM medium containing 0-200 µL of fetal bovine serum (FBS) saturated with pristane (FBS/pristane), or with FBS alone. Annexin-V staining was measured by flow cytometry after 24-h (left) or 48-h (right) of culture. Data are representative of two independent experiments. (**E**), RAW264.7 cells were cultured for 24-h in the presence of rapamycin (50 ng/mL in DMEM+10% FBS, Rap), pristane (in 5% pristane-saturated FBS plus 5% pristane-free FBS, Pris), or medium alone [10% FBS, (-)]. Western blot was carried out using anti-LC3 and anti-tubulin antibodies (as a loading control). Positions of LC3B-I and LC3B-II bands are indicated. Representative of three independent experiments.

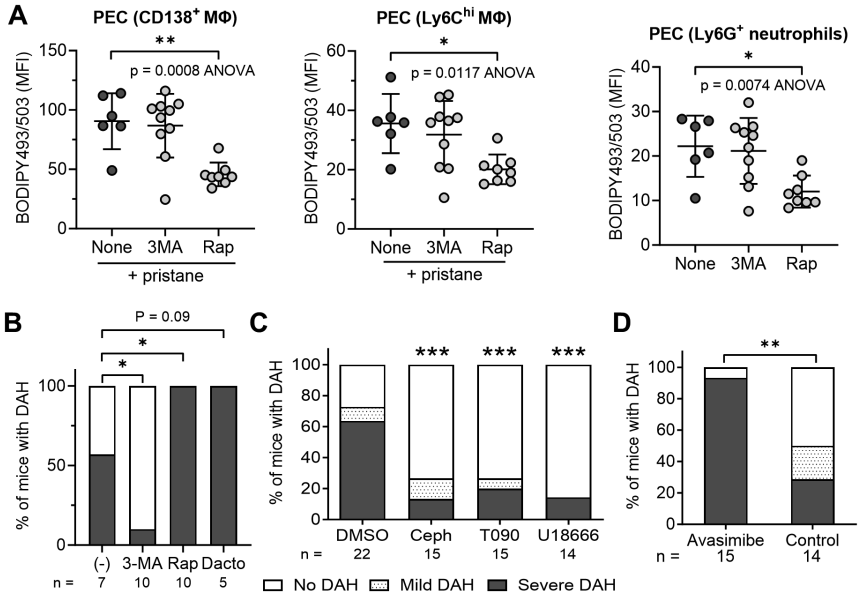

Figure 3. *Altered lipid homeostasis in pristane-induced DAH.* (**A-B**), B6 mice were treated with pristane alone (-) or with pristane plus 3-methyladenine (3MA), rapamycin (Rap), or dactolisib (Dacto). After 14-d, peritoneal exudate cells (PECs) were stained with BODIPY 493/503 plus anti-CD11b, CD138, Ly6C, and Ly6G antibodies and analyzed by flow cytometry. (**A**), Mean fluorescence intensity (MFI) of BODIPY493/503 staining in individual cell subsets. *, $P < 0.05$; ** $P < 0.01$ (ANOVA, Dunnett's multiple comparison test). (**B**), percentage of mice in each group with diffuse alveolar hemorrhage (DAH). (**C**), B6 mice were treated pristane plus cepharanthine (Ceph), T0901317 (T090), or U18666A in DMSO, or vehicle alone (DMSO) and the frequencies of severe or mild DAH at day-14 were determined. (**D**), B6 mice were treated with pristane plus avastimibe or with pristane alone (Control) and percentages of mice with DAH at were determined at day-14. (B-D), **, $P < 0.01$; *** $P < 0.001$ (Chi-square). Numbers of mice (n) are indicated at the bottom (B-D).

mediated reverse cholesterol transport (T0901317) or sequestering free cholesterol inside lysosomes (U18666A, cepharanthine), whereas blocking the esterification of cytoplasmic free cholesterol by ACAT inhibition (avasimibe) increased disease severity. Together, these observations suggest that high levels of cytoplasmic free cholesterol enhance susceptibility to DAH.

Effect of U18666A is interferon-independent

Pristane induces a type I interferon (IFN) signature, whereas MO treatment does not.[2] Mice lacking either the type I IFN receptor (*Ifnar1*-/-) or IFNγ (*Ifng*-/-) are protected from the induction of lupus autoantibodies and lupus nephritis.[2] In contrast, B6-*Ifnar1*-/- mice are fully susceptible to the induction of DAH. The susceptibility of B6-*Ifng*-/- mice to pristane-induced DAH has not been studied.

Cholesterol 25-hydroxylase (Ch25h), which converts cholesterol to 25-hydroxycholesterol (25HC) and has a role in inflammation and the regulation of LXRs,[33] is upregulated in Mϕ by both type I (e.g. IFNα) and type II (IFNγ) via Stat1.[34] We asked whether blocking Npc1 or stimulating LXR activity blocks the induction of type 1 and type 2 IFN stimulated genes by pristane.

In PECs from pristane-treated mice, U18666A, cepharanthine, and T0901317 did not significantly affect the expression of the type I IFN regulated genes *Mx1*, *Irf7*, and *Isg15* (Figure 4A). Pristane induced expression of the IFNγ regulated genes *Cxcl10* and *Irf1* (Figure 4B). However, in PECs from pristane-treated mice, U18666A did not affect the expression of *Cxcl10, Irf1* or the IFNα/IFNγ-regulated *Ch25h* gene[35] (Figure 4C). In peripheral blood cells, pristane treatment reduced *Ch25h*, but as in PECs, U18666A did not restore expression to normal levels (Figure 4D).

Ch25h-regulated 25HC production in monocyte-derived Mϕ recruited to the inflamed lung promotes the resolution of lung injury, but 25HC production by lung endothelial cells stimulates lipopolysaccharide (LPS)-induced inflammatory cytokine production, ER stress, and endothelial leak [36]. The dominant effect of 25HC is amplification of LPS-induced lung injury and endothelial leak. U18666A treatment reduced *Ch25h* expression in lung tissue from pristane-treated mice, suggesting that it might modulate lung inflammation (Figure 4E).

Although Npc1 inhibition had little effect on *Ch25h* expression in peripheral blood cells, both U18666A and cepharanthine potently blocked the expression of TremL4 staining on the surface of blood monocytes (Figure 4F). TremL4 is a protein that amplifies proinflammatory signaling[37,38] and is expressed at high levels on circulating $CD138^+$ monocytes in mice with pristane-induced DAH.[4] It may serve as a marker for $CD138^+Ly6C^-$ monocytes that have lost the capacity to promote vascular repair. Consistent with prior studies in pristane-treated B6 mice,[4] TremL4 expression was higher on $CD138^+$ monocytes than the $Ly6C^{lo}CD138^-$ or $Ly6C^{hi}CD138^-$ monocyte subsets (Figure 4F). Surface staining of all three subsets was substantially reduced by U18666A or cepharanthine treatment.

U18666A and cepharanthine sequester cholesterol within the lysosomes, lowering the cytoplasmic levels of free cholesterol and 25-HC.[31,39] Since high cytoplasmic levels of free cholesterol can induce ER stress and apoptosis,[40] we examined the effect of NPC1 inhibition on pristane-induced ER stress.

U18666A blocks induction of ER stress markers in lung but not myeloid cells

Pristane treatment activates the UPR and Golgi/ER stress is seen in pulmonary endothelial cells from B6 (susceptible to DAH) but not BALB/c (resistant to DAH) mice.[8] Enhancing ER stress by treating with pristane + low-dose

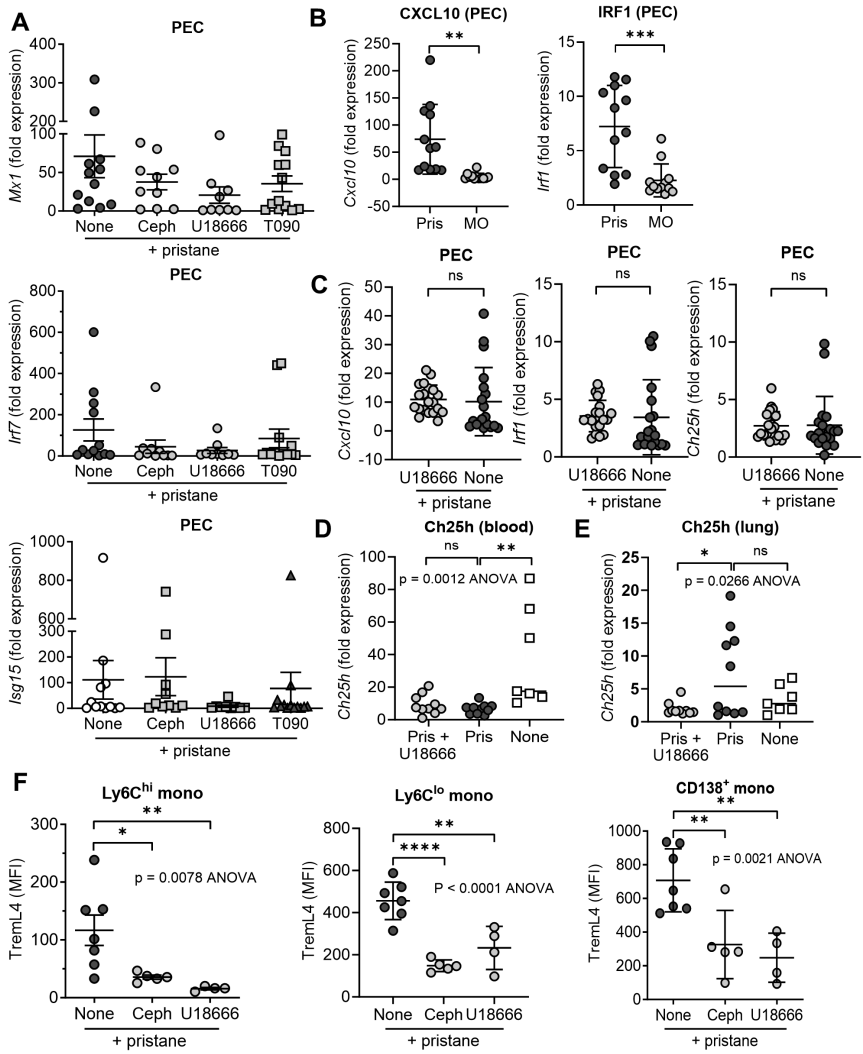

Figure 4. *Effect of U18666A and cepharanthine is interferon-independent.* Mice were treated with pristane + cepharanthine (Ceph), U18666A (U18666), or T0901317 (T090) or pristane without any other addition (None) and gene expression was analyzed 14-d later. (**A**), expression of interferon stimulated genes *Mx1, Irf7*, and *Isg15* in peritoneal exudate cells (PECs). Differences were not significant (ANOVA). (**B**), IFNγ regulated gene expression (*Cxcl10* and *Irf1*) in PECs from mice treated with pristane (Pris) or mineral oil (MO). **, P < 0.01; *** P < 0.001, (Student t-test). (**C**), *Cxcl10, Irf1*, and *Ch25h* expression in PECs from pristane-treated mice concomitantly treated with U18666A or vehicle (-). ns, not significant (Student t-test). (**D-E**), expression of *Ch25h* in peripheral blood mononuclear cells (**D**) and total lung tissue (**E**) from mice treated with pristane (Pris) or pristane+U18666A, vs. controls that did not receive pristane or U18666A (None). *, P < 0.05; **, P < 0.01; **** P < 0.0001; ns, not significant, (ANOVA, Dunnett's multiple comparison test). (**F**), Peripheral blood cells were analyzed by flow cytometry 14-d after pristane treatment. Cells were stained with anti-CD11b, Ly6C, CD138, Ly6G, and TremL4

thapsigargin causes DAH in BALB/c mice. Although classically induced by the accumulation of unfolded or misfolded proteins in the ER, cholesterol accumulation in the ER membrane also potently induces ER stress via the IRE1 pathway.[9,41]

We examined the effect of U18666A on the expression of Golgi/ER stress markers in PECs and lung. The Golgi marker *Copa* is low/absent in COPA syndrome, a human genetic disorder with autoimmune features characterized by DAH and ER stress,[42] and also is markedly decreased in pristane-induced DAH.[8] *Copa* expression in PECs was unaffected by treating with cepharanthine, U18666A, or T0901317 along with pristane (Figure 5A). In contrast, expression in the lung was restored to normal by co-administering U18666A along with pristane (Figure 5B). The ER stress markers *Hspa5* (BiP) and *Ddit3* (CHOP) increase in lung from pristane-treated mice with DAH.[8] *Hspa5* expression in PECs from pristane-treated mice was unaffected by concomitant treatment with cepharanthine, U18666A, or T0901317 (Figure 5C). U18666A also did not normalize *Hspa5* expression in lung from pristane-treated mice (Figure 5D). In pristane-treated mice, *Ddit3* expression in PECs was unaffected by cepharanthine, U18666A, or T0901317 (Figure 5E), but U18666A normalized *Ddit3* expression in the lung (Figure 5F). Cholesterol trafficking to the ER activates *Ddit3*/CHOP, resulting in ER stress-induced apoptosis.[43,44] Our data are consistent with reports that U18666A protects cells from apoptosis induced via LMP[45] and from cholesterol-induced ER stress.[3°] However, although pristane induces apoptosis in myeloid cells (Figure 2D), it may cause cell death by a different pathway in myeloid cells vs. lung.

U18666A blocks differentiation of inflammatory CD138$^+$ monocytes/Mϕ

Cholesterol promotes proinflammatory Mϕ polarization and atherosclerosis.[46,47] Since pristane-induced DAH is prevented by depleting monocytes/Mϕ with clodronate liposomes or blocking the recruitment of monocytes to the lung (*Ccr2*-/- mice),[3,8] we investigated the effects of U18666A, cepharanthine, and T0901317 on myeloid cells. Three monocyte subsets appear in the blood after pristane treatment, two of which (Ly6C^{hi}Ly6G$^-$CD11b$^+$CD138$^-$ and Ly6C^{l}°Ly6G$^-$CD11b$^+$CD138$^-$) also are seen in the circulation of MO-treated mice.[4]

monoclonal antibodies. TremL4 staining (mean fluorescence intensity, MFI) is shown on the CD11b$^+$Ly6G$^-$CD138$^-$Ly6C^{hi} monocytes (Ly6C^{hi} mono, left), CD11b$^+$Ly6G$^-$CD138$^-$Ly6C^{lo} monocytes (Ly6C^{lo} mono, center), and CD11b$^+$Ly6G$^-$CD138$^+$Ly6C^{neg} monocytes (CD138$^+$ mono, right) subsets. *, $P < 0.05$; **, $P < 0.01$; **** $P < 0.0001$; ns, not significant, (ANOVA, Dunnett's multiple comparison test).

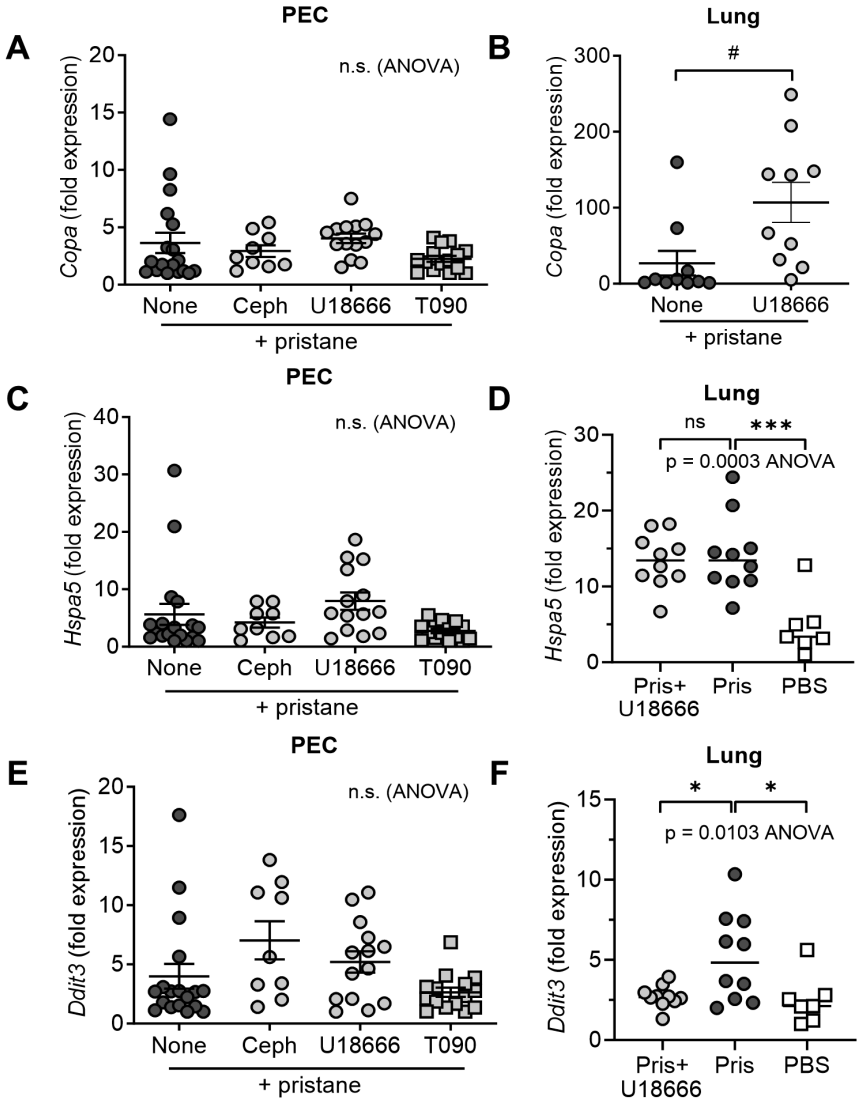

Figure 5. *U18666A blocks induction of ER stress markers in the lung.* Mice were treated with pristane + cepharanthine (Ceph), U18666A (U18666), or T0901317 (T090), pristane without any other addition (None), or PBS (no pristane). Gene expression was analyzed 14-d later. (**A, C, E**), gene expression in peritoneal exudate cells (PEC); (**B, D, F**), gene expression in lung. (**A-B**), expression of *Copa*; (**C-D**), expression of *Hspa5* (Bip); (**E-F**), expression of *Ddit3* (CHOP). # $P < 0.05$ (Student t-test). *, $P < 0.05$; *** $P < 0.001$, ns, not significant (ANOVA, Dunnett's multiple comparison test).

The percentages of these cells were unaffected by administering cepharanthine, U18666A, or T0901317 to pristane-treated mice (Figure 6A). In contrast, circulating $Ly6C^{lo}Ly6G^{-}CD11b^{+}CD138^{+}$ cells ("$CD138^{+}$ monocytes")

increase in pristane-treated mice with DAH, but not in MO-treated mice,[4] and were nearly absent in mice receiving cepharanthine or U18666A along with pristane, but were unaffected by T0901317 (Figure 6A). Circulating $Ly6G^{+}CD11b^{+}$ neutrophils were unaffected by T0901317, but increased in mice treated with pristane plus cepharanthine or U18666A.

As it is technically challenging to quantify subsets of bone marrow-derived myeloid cells in lung tissue, we examined Mϕ generated from monocytes recruited to the peritoneum of pristane-treated mice. In PECs, cepharanthine and U18666A decreased $Ly6C^{lo}CD138^{+}$ and $Ly6C^{lo}CD138^{-}$ Mϕ but did not affect the $Ly6C^{hi}$ subset (Figure 6B). T0901317 reduced peritoneal $CD138^{+}$ Mϕ. Cepharanthine, U18666A, and T0901317 all increased the percentage of peritoneal $Ly6G^{+}$ neutrophils in pristane-treated mice (Figure 6B). Thus, drugs that sequester cholesterol in lysosomes impaired the generation of non-classical ($Ly6C^{lo}CD138^{+}$ and $Ly6C^{lo}CD138^{-}$) monocytes/Mϕ, but had little effect on classical ($Ly6C^{hi}$) monocytes/Mϕ.

Effect of pristane on genes that regulate cholesterol accumulation

We next examined whether pristane alters the expression of genes involved in cholesterol transport. Pristane treatment decreases LXR-regulated Abca1 expression and it is restored and DAH is prevented by treating with a synthetic LXR agonist.[5] RNA-Seq analysis revealed increased levels of *Npc1* and *Npc2* mRNA in peritoneal $Ly6C^{hi}$ Mϕ from pristane vs. MO treated mice (Figure 7A-B). A smaller effect (not statistically significant) was seen in peritoneal $CD138^{+}$ Mϕ. Expression of the neutral cholesterol ester hydrolase 1 (*Nceh1*) gene, an ER-resident enzyme catalyzing the de-esterification of cholesterol, also was higher in both $Ly6C^{hi}$ and $CD138^{+}$ peritoneal Mϕ from pristane- vs. MO- treated mice (Figure 7C). Like Npc1 and Npc2, increased levels of Nceh1 could promote free cholesterol accumulation if re-esterification or reverse cholesterol transport is impaired.[40] In contrast, expression levels of *Ldlr* (mediates uptake of low-density lipoproteins), *Cd36* (mediates uptake of oxidized LDL), *Ptafr* (a co-factor for CD36), *Lipa* (encodes LAL), *Acat1*, and *Hmgcr* (rate-limiting enzyme in cholesterol biosynthesis) were similar in pristane- vs. MO- treated $Ly6C^{hi}$ and $CD138^{+}$ Mϕ (Figure 7D-I). The differential expression of *Npc1, Npc2*, and *Nceh1* mRNA in PECs from pristane- vs. MO- treated mice was confirmed by qPCR (Figure 7J).

Effect of U18666A on lysosomal enzymes

Pristane-induced lipid accumulation and increased autophagosome staining along with reduced neutral lipid staining in mice receiving rapamycin plus pristane (Figures 1-2) are consistent with the transport of neutral lipids to lysosomes and hydrolysis by LAL.[23] LAL is the only lysosomal enzyme known

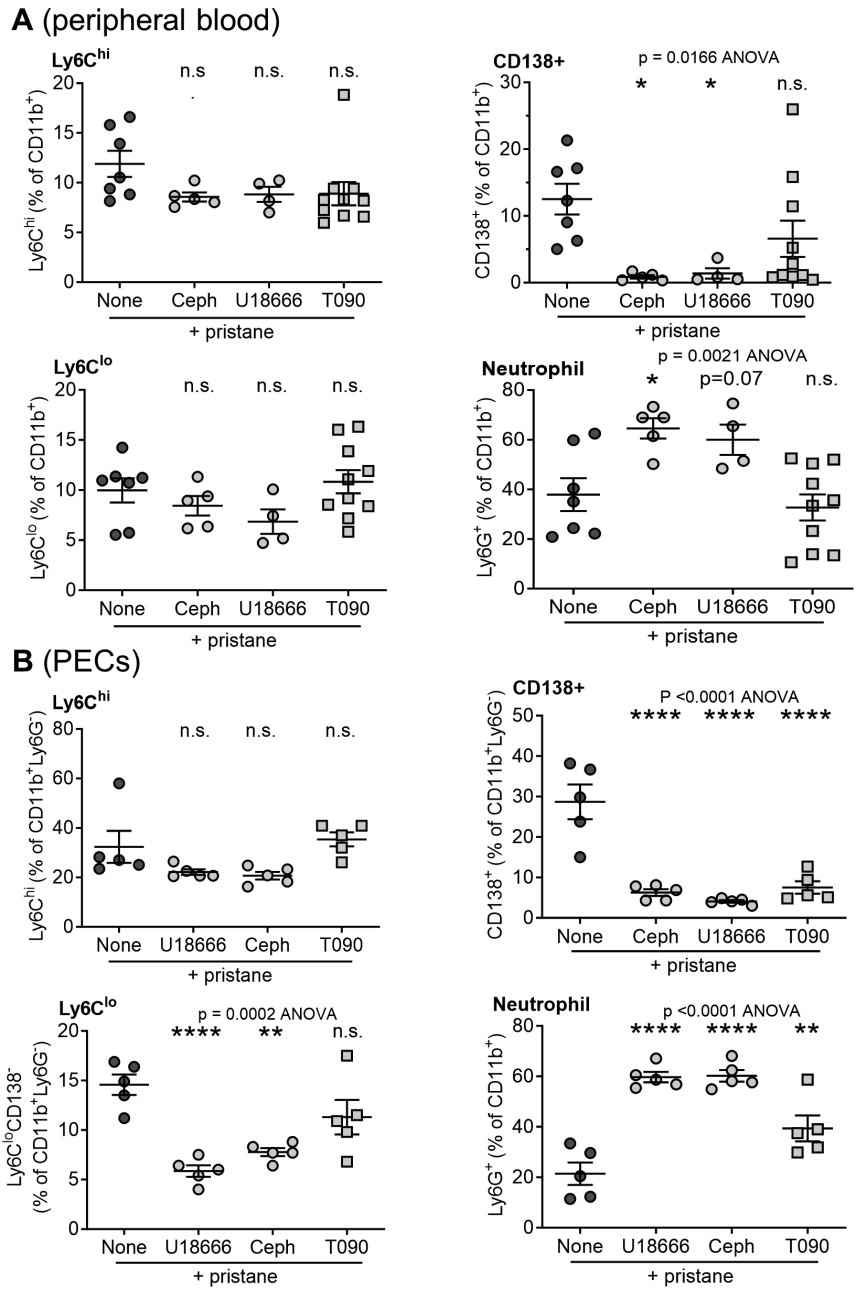

Figure 6. *U18666A blocks differentiation of inflammatory CD138$^+$ monocytes/Mϕ.* Mice were treated with pristane + cepharanthine (Ceph), U18666A (U18666), or T0901317 (T090) or pristane without any other addition (None) and myeloid subsets were analyzed 14-d later by flow cytometry. Data for each CD11b$^+$ subset (Ly6C^{hi}CD138$^-$, Ly6C$^-$CD138$^+$, Ly6C^{lo}CD138$^-$, and Ly6G$^+$) are expressed as the % of total CD11b$^+$ cells (A), peripheral blood (circulating) cells; (B), peritoneal exudate cells (PECs). *, $P < 0.05$; **, $P < 0.01$; **** $P < 0.0001$, ns, not significant (ANOVA, Dunnett's multiple comparison test).

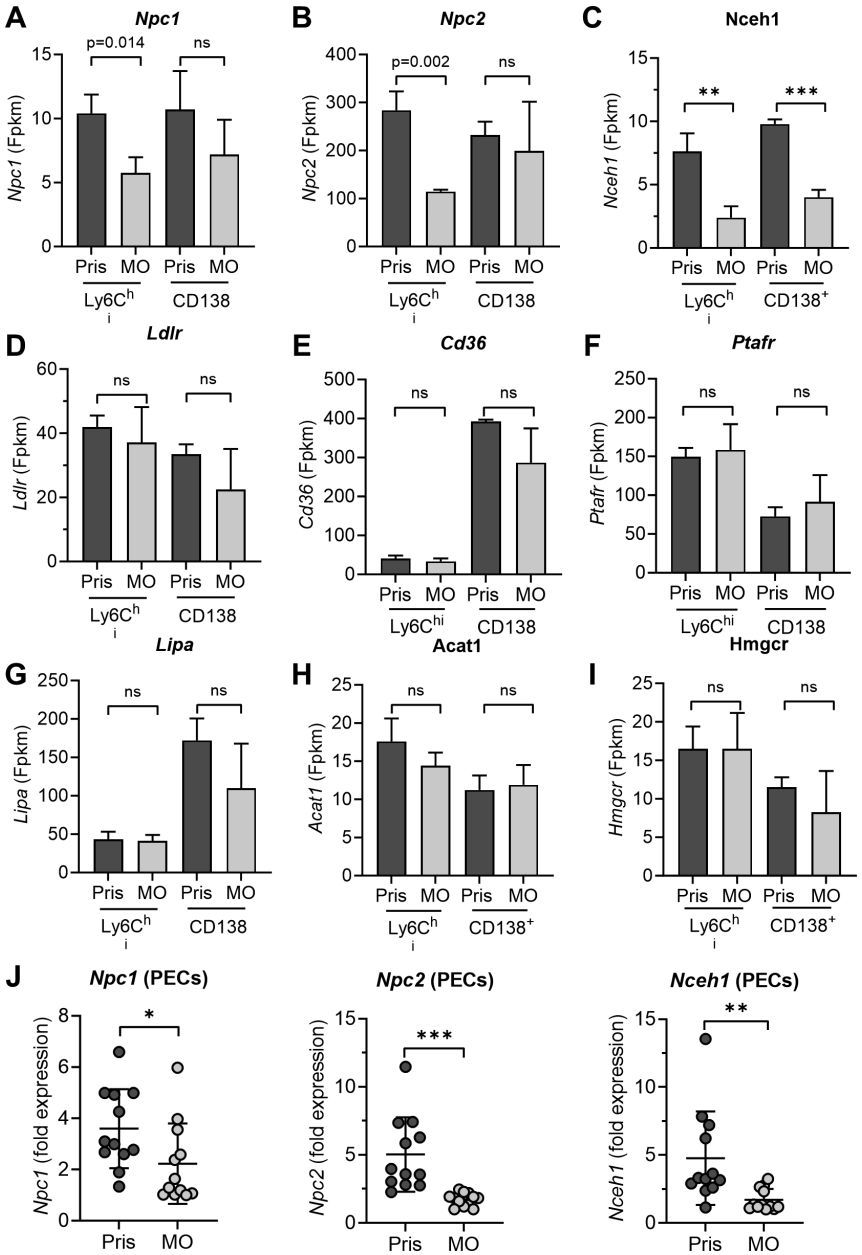

Figure 7. *Increased Npc1, Npc2, and Nceh1 expression in pristane-treated mice.* Mice were treated with pristane (Pris) or mineral oil (MO) and 14-d later, gene expression was evaluated in peritoneal CD11b^{+}Ly6C^{hi}CD138^{-} and CD11b^{+}Ly6C^{hi}CD138^{-} Mϕ by RNA-Seq (**A-I**) or in total PECs by qPCR (**J**). (**A-I**), Relative expression of genes encoding proteins involved in the regulation of intracellular lipid homeostasis (RNA-Seq): *Npc1, Npc2, Nceh1, Ldlr, Cd36, Ptafr, Lipa, Acat1*, and *Hmgr*. (**J**), Expression of *Npc1, Npc2*, and *Nceh1* in PECs from pristane and MO treated mice (qPCR). Fpkm, fragment per kilobase million. *, $P < 0.05$; **, $P < 0.01$; *** $P < 0.001$, ns, not significant (Student t-test).

to degrade the cholesterol esters in LDL and lipid droplets, yielding free cholesterol and fatty acids.[25,48,49] Free cholesterol is transported out of the lysosome by Npc1 and Npc2.[28,29] In *Npc1-/-* mice free cholesterol accumulates in the lysosomes. In contrast, cholesterol ester accumulates in the lysosomes of mice and humans with LAL mutations and foamy Mϕ fill the alveoli, though DAH does not occur.[48,50]

The effect of pristane treatment on LAL activity was examined. In peritoneal cells from MO-treated controls, LAL enzyme activity was detected in both $CD138^{+}Ly6C^{lo}$ and $CD138^{-}Ly6C^{-}$ Mϕ (Figure 8A). Activity was low in $Ly6G^{+}$ neutrophils. LAL activity was substantially lower in $CD138^{+}$ and $CD138^{-}$ Mϕ from pristane- vs. MO- treated mice (Figure 8A). U18666A did not normalize LAL activity in pristane treated mice (Figure 8B). The low level of LAL activity and the high *Plip2* expression suggests that lysosomal degradation of lipid droplets may be impaired in pristane-treated mice. Interestingly, although LAL is regulated primarily at the transcriptional level,[48] *Lipa* mRNA expression (qPCR) was somewhat higher in pristane- vs. MO- treated mice whereas LAL activity was very low, (Figure 8C, A), suggesting that pristane might downregulate LAL enzyme activity post-transcriptionally. U18666A lowered Lipa mRNA expression (Figure 8C) without affecting LAL enzyme activity (Figure 8B).

Cathepsins are endolysosomal proteases that are dysregulated in a variety of human diseases and play an important role in viral pathogenesis.[51] and apoptosis[52] LMP releases cathepsins into the cytoplasm, promoting apoptosis.[15] Microinjection of cathepsin D induces caspase-dependent apoptosis, which can be blocked using the cathepsin D inhibitor pepstatin-A.[53,54] *Ctss* (cathepsin S), *Ctsd* (cathepsin D), *Ctsl* (cathepsin L), and *Ctsk* (cathepsin K) all were expressed at higher levels in PECs from pristane- vs. MO-treated mice (Figure 8D). Lysosomal cholesterol accumulation resulting from U18666A treatment prevents LMP by increasing lysosomal stability.[16] Administration of U18666A also decreased *Ctss, Ctsd*, and *Ctsk* expression, but not *Ctsl*, to control levels in pristane-treated mice (Figure 8E). The increased levels of lysosomal cathepsin mRNAs were accompanied by increased cathepsin K enzyme activity in peritoneal $CD138^{+}$ and $CD138^{-}$ Mϕ as well as neutrophils from pristane-treated mice (Figure 8F). The highest cathepsin K activity was seen in $CD138^{+}$ PECs. Cathepsins S, D, and K all are implicated in the pathogenesis of lupus.[55–58] These observations suggest that pristane treatment causes lysosome dysfunction and that U18666A may protect mice from DAH by increasing lysosomal cholesterol content and preventing LMP as well as by reducing the levels of the lysosomal proteases released during LMP.

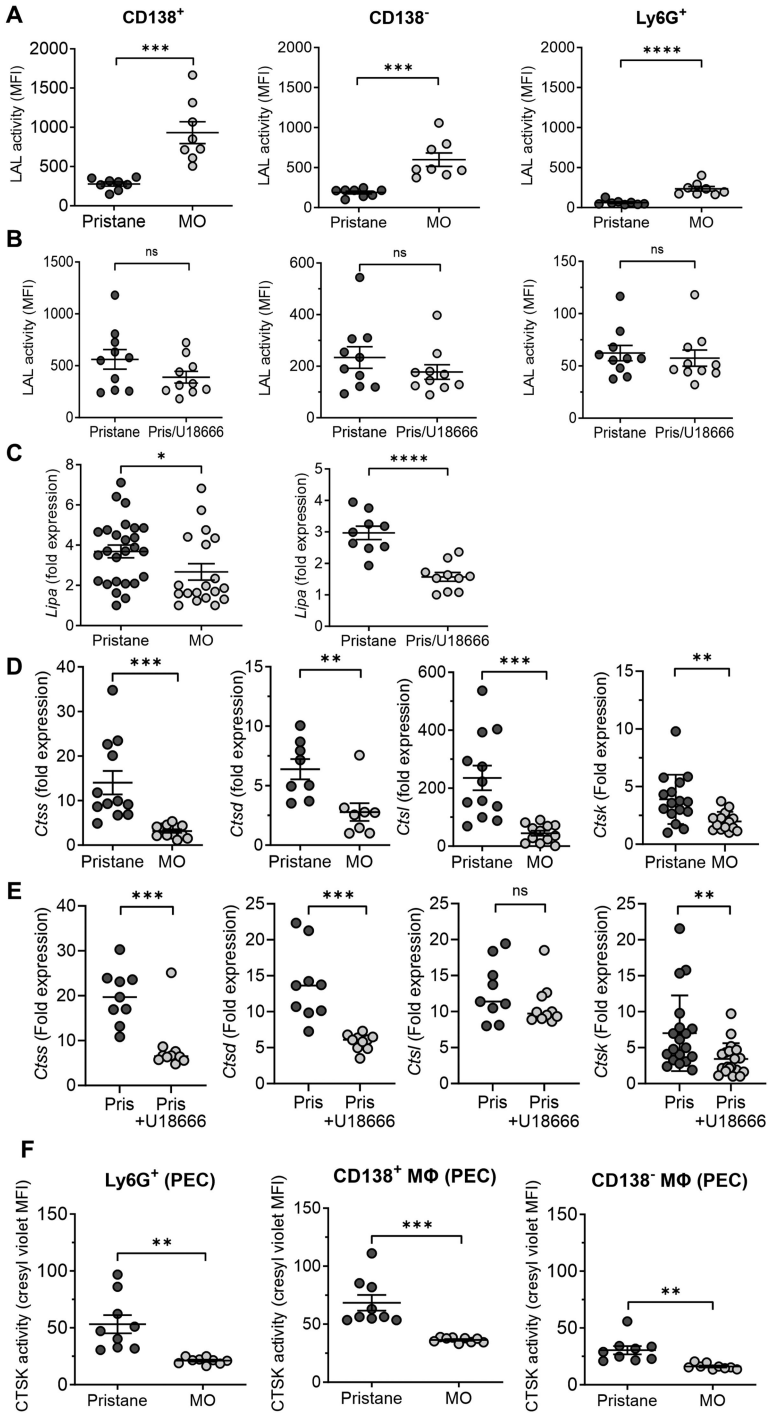

Figure 8. *Effect of U18666A on lysosomal enzymes.* (**A**), B6 mice were treated with pristane or mineral oil (MO) and lysosomal acid lipase (LAL) enzyme activity was

Lysosome size/volume increases in pristane-exposed Mϕ and is normalized by U18666A

Lysosomes are critical to the cellular stress response[59] and increased lysosomal size promotes LMP and LDCD.[15] We assessed lysosome biogenesis by measuring lysosome-associated membrane glycoprotein 1 (LAMP1/CD107a).[60] Cathepsin D and LAMP1 are both regulated by TFEB (transcription factor EB), the master regulator of genes encoding lysosomal membrane proteins and hydrolases.[60,61] Expression of both was higher in $CD138^+$ Mϕ from pristane- vs. MO- treated mice (Figures 8E and 9A). Increased lysosomal volume (a function of the size and number of lysosomes), a key indicator of lysosome biogenesis,[60] was assessed using LysoTracker green. Pristane treatment dramatically increased LysoTracker green staining (Figure 9B), whereas lysosomal pH did not change as determined by LysoSensor staining (Figure 9C). In RAW264.7 (murine Mϕ) cells, pristane, but not MO, induced a dose-dependent increase in LAMP-1/CD107a staining (Figure 9D). Consistent with high levels of LAMP-1 and cathepsin D, *Tfeb* expression was higher in PECs from pristane- vs. MO- treated mice (Figure 9E).

Pristane also increased lysosomal volume (LysoTracker staining) in RAW 264.7 cells (Figure 9F, left, unshaded bars). Lysosome volume was reduced in a dose-dependent manner by adding U18666A to the culture medium along with pristane, whereas U18666A had no effect on lysosome volume in cells cultured with carrier alone (Figure 9F, left). As in $CD138^+$ Mϕ, lysosomal pH was unaffected by adding U18666A to pristane-treated RAW264.7 cells (Figure 9F, right). These data indicate that the lysosome biogenesis pathway is activated by pristane treatment, most likely through the activity of TFEB, and that this may be reversed by the accumulation of free cholesterol in the lysosomes (U18666A treatment). Although *Tfeb* gene expression increased in pristane-treated mice, TFEB activity is regulated primarily through

measured at day-14 in $CD11b^+CD138^+Ly6G^-$ Mϕ, $CD11b^+CD138^-Ly6G^-$ Mϕ, and $CD11b^+CD138^-Ly6G^+$ neutrophils. (**B**), B6 mice were treated with pristane alone (-) or pristane + U18666A. Lysosomal acid lipase (LAL) enzyme activity was measured at day-14 in $CD11b^+CD138^+Ly6G^-$ Mϕ, $CD11b^+CD138^-Ly6G^-$ Mϕ, and $CD11b^+CD138^-Ly6G^+$ neutrophils. (C-D), mRNA expression (qPCR) at day-14 in total PECs from mice treated with pristane or MO or pristane+U18666A. (**C**), lysosomal acid lipase (*Lipa*) expression. (**D**), cathepsin S (*Ctss*), cathepsin D (*Ctsd*), cathepsin L (*Ctsl*) and cathepsin K (*Ctsk*) expression. (**E**), expression of *Ctss, Ctsd, Ctsl*, and *Ctsk* in total PECs from B6 mice treated with pristane alone (Pris) or pristane + U18666A. F, CTSK enzyme activity 14-d after pristane or MO treatment in peritoneal exudate cell (PEC) subsets: $L6G^+$ neutrophils (left), $Ly6G^-CD11b^+CD138^+$ Mϕ (middle), and $Ly6G^-CD11b^+CD138^-$ Mϕ (right). *, $P < 0.05$; **, $P < 0.01$; *** $P < 0.001$; **** $P < 0.0001$; ns, not significant (Student t-test).

dephosphorylation.[60] Unfortunately, due to the low abundance of TFEB, it is reportedly difficult to evaluate the subcellular distribution by immunofluorescence.[60]

Chloroquine, chlorpromazine, and other cationic amphiphilic (lysosomotropic) drugs are sequestered in lysosomes, increasing lysosomal volume (LysoTracker), cathepsin activity, and LAMP1 staining.[62,63] Most enhance autophagy but chloroquine inhibits it.[62] In addition, these drugs can alter lipid metabolism and/or transport at therapeutic concentrations, resulting in lysosomal neutral phospholipid and cholesterol accumulation and inflammation ("drug-induced phospholipidosis").[64] The ability of these drugs to increase lysosomal volume correlates with their ability to intercalate into the lysosomal membrane,[63] resulting in increased LMP.[64] Pristane also can intercalate into the cell membrane.[65] Consistent with the flow cytometry data, pristane exposure increased the intensity of LysoTracker staining in live RAW264.7 cells by confocal microscopy (Figure 9G). Individual lysosomes in pristane-treated cells appeared larger and brighter than those in cells incubated in medium alone. Lysosomes in pristane-treated cells appeared similar to those in cells incubated with chloroquine, which causes lysosomal enlargement/swelling and the intensity of LysoTracker staining per cell in pristane- vs. chloroquine- treated cells was similar (Figure 9G). Pristane-treated RAW264.7 cells also were stained with BODIPY493/503 plus anti-LAMP1 antibodies (Figure 9H). Consistent with the flow cytometry staining (Figure 1), BODIPY fluorescence was more prominent in pristane-treated cells vs. cells incubated with medium alone. BODIPY fluorescence did not co-localize with $LAMP1^+$ lysosomes. However, the relationship of lysosome staining to BODIPY staining could not be characterized further due to the previously described,[66] alteration of lysosomal morphology by paraformaldehyde fixation.

Discussion

Severe DAH with pulmonary vasculitis complicating pristane-induced lupus [2] is prevented by depleting monocytes/Mϕ or by LXR agonist (T0901317) therapy.[3] Although T0901317 impairs inflammatory responses by promoting M2-like monocyte/Mϕ polarization,[5,6] it also enhances reverse cholesterol transport by increasing *Abca1* expression.[6,7] The present study examined the role of lipid regulation in DAH.

Lung Mϕ in mice with DAH contained numerous lipid droplets (Figure 1A). Cytoplasmic neutral lipid staining and autophagosome staining increased (Figure 1B-E). Activation of autophagy by rapamycin treatment decreased neutral lipid accumulation but exacerbated pristane-induced DAH, whereas DAH was milder when autophagy was inhibited by 3MA (Figure 3). Drugs that inhibit NPC1 (U18666A, cepharanthine) sequester cholesterol within lysosomes

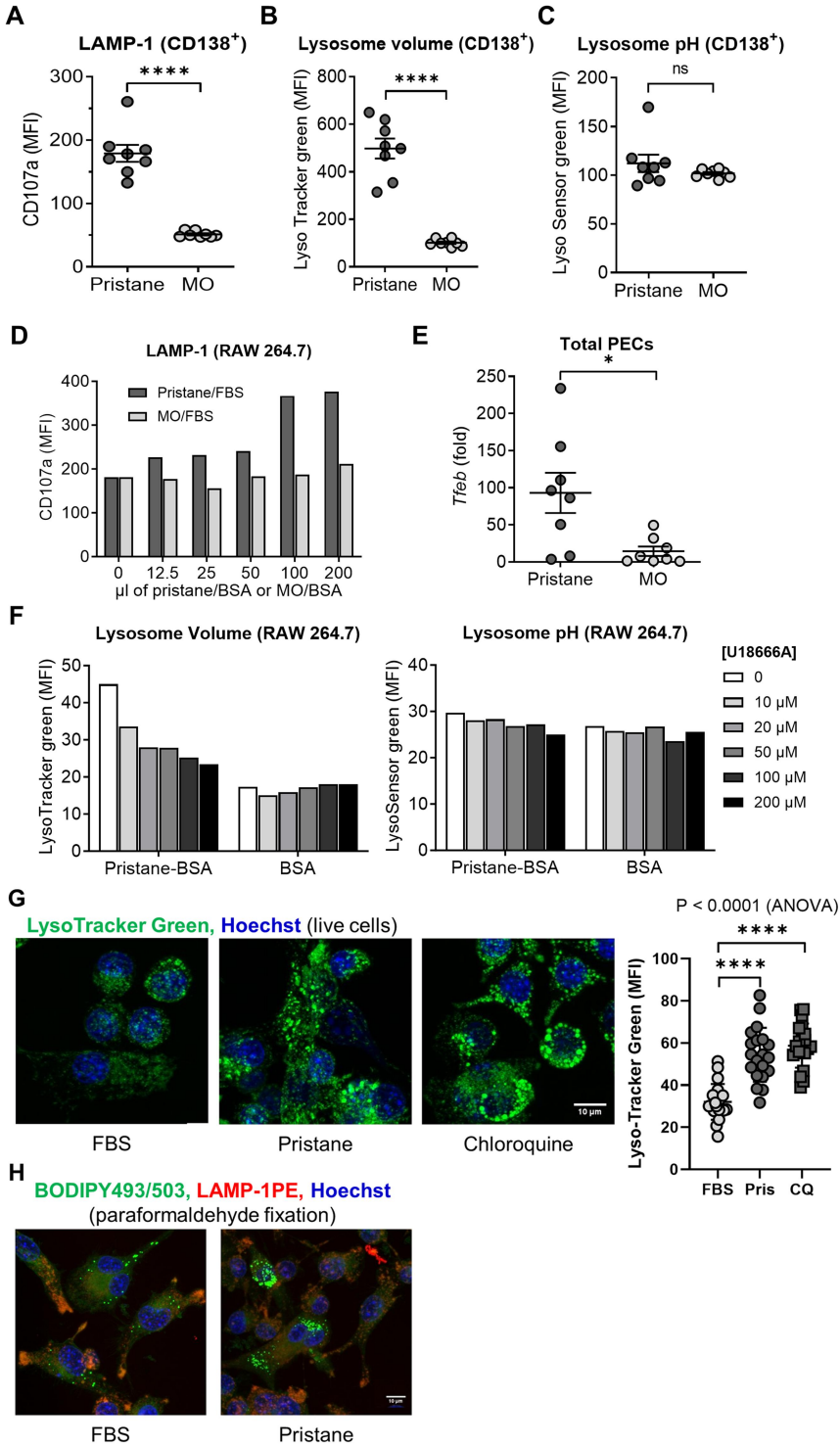

Figure 9. *Pristane treatment increases lysosome size in Mϕ.* (**A**), B6 mice were treated with pristane or mineral oil (MO) and 14-d later, cells were stained with anti-CD11b, CD138,

and potently blocked the onset of DAH (Figure 3). Conversely, ACAT inhibition, which can raise cytoplasmic free cholesterol,[67] exacerbated DAH (Figure 3).

Pristane activated the lysosome biogenesis pathway, probably by increasing TFEB (Figure 9) and this was blocked by U18666A. TFEB enhances transcription of cathepsins, which were upregulated in pristane-treated mice and blocked by U18666A (Figure 8). Pristane treatment also increased cathepsin enzyme activity and lysosomal size/number (Figures 8F,9). Finally, in the target organ (lung), but not PECs, pristane-induced expression of ER stress markers *Copa* and *Ddit3* (CHOP) was normalized by U18666A treatment (Figure 5). Together, the data suggest that pristane causes cellular accumulation of neutral lipid, which is transported to the lysosomes by autophagosomes. The resulting lysosomal enlargement may promote LMP and cytoplasmic leakage of cathepsins in myeloid cells, which migrate to the lung causing ER stress in the target organ, possibly due to LDCD of myeloid cells and the release of DAMPs, as suggested by the induction of myeloid cell apoptosis by pristane (Figure 2D). Consistent with that model, enlarged Mϕ undergoing apoptosis are demonstrable in the lung of pristane-treated mice by TUNEL staining.[3] We hypothesize that raising lysosomal free cholesterol by treating with U18666A or cepharanthine stabilizes the lysosomes, protecting them from LMP and LDCD.

---

and Ly6G antibodies. A-C, Anti-CD107a (LAMP-1) staining (mean fluorescence intensity, MFI) (**A**), LysoTracker green (lysosome volume, MFI) (**B**), and LysoSensor green (lysosome pH, MFI) (**C**) in $CD11b^{+}CD138^{+}Ly6G^{-}$ cells was determined by flow cytometry. (**D**), RAW264.7 cells were cultured for 24-h with pristane or MO [0-200 µL of saturated pristane or MO solution in 100 mg/ml bovine serum albumin (BSA) in a final volume of 2 ml culture medium]. Cells were stained with anti-CD107A (LAMP-1) antibodies and analyzed by flow cytometry (MFI). Data are representative of two independent experiments. (**E**), *Tfeb* gene expression (qPCR) in total PECs from mice treated for 14-d with pristane or MO. (**F**), RAW264.7 cells were cultured with pristane [100 µL of saturated pristane solution in 100 mg/ml bovine serum albumin (BSA) or BSA alone in a final volume of 2 ml DMEM+10% FBS] plus U18666A (0-200 µM). After 24-h, lysosome volume (LysoTracker green, MFI) and lysosomal pH (LysoSensor green, MFI) was determined by flow cytometry. Data are representative of two independent experiments. *, $P < 0.05$; **** $P < 0.0001$, ns, not significant (Student t-test). (**G**), Confocal imaging of lysosomes in RAW264.7 cells treated with pristane (Pris) in 10% fetal bovine serum (FBS) or chloroquine (CQ) in 10% FBS for 20-h or with 10% FBS alone. Cells were stained with LysoTracker Green DND 26 (green) and Hoechst 33342 (blue) to visualize DNA in nuclei. Original magnification X60. White bar, right panel, indicates 10 µm. *Right*, LysoTracker staining (mean fluorescence intensity, MFI, per cell) was determined using Fiji Software and analyzed by one-way ANOVA (representative of 2 experiments). **** $P < 0.0001$, Dunnett's multiple comparison test. (**H**), Confocal imaging of BODIPY493/503 (green) was performed on unfixed RAW264.7 cells treated with pristane-10% FBS or FBS alone. Anti-LAMP1-phycoerythrin staining (red) and Hoechst 33342 (DNA) staining was carried out after paraformaldehyde fixation and permeabilization. Original magnification X60. White bar, right panel, indicates 10 µm.

Neutral lipid accumulates in monocytes/Mϕ after pristane treatment

Lipid droplets are dynamic, phospholipid monolayer-enclosed, storage organelles for neutral lipid derived from the ER.[18] Sequestration of lipids within these structures prevents lipotoxicity.[68] The coatomer complex I (COPI), which is implicated in the pathogenesis of DAH in both COPA syndrome patients and pristane-induced lupus,[8,42] regulates the association of lipid droplets with the ER.[18,69] Under conditions of nutrient deprivation, lipid droplets are taken up by autophagosomes and the stored lipids are degraded in lysosomes by LAL (lipophagy).[2,68] Impaired lipophagy leads to the formation of foamy Mϕ, ER stress, and cell death in human diseases.[9,23,26]

H&E, Nile red, and BODIPY staining revealed increased neutral lipid in the cytoplasm of monocytes/Mϕ from pristane-treated mice vs. controls (Figure 1). The lipid droplet protein perilipin-2/adipophilin (Plin2) is expressed rapidly in lipid-overloaded cells, serving as a marker for lipid loading [70]. Thus, the high level of *Plin2* in PECs from pristane-treated mice (Figure 1G) is consistent with lipid overload.

After peritoneal injection, pristane is widely distributed in tissues including the lung [3], probably due to uptake by peritoneal lymphatics draining into the thoracic duct. Pristane is highly hydrophobic and may associate with amphipathic structures in the blood. Similarly, squalene, another hydrophobic molecule that induces lupus in mice,[71] associates with LDL in the serum.[72] It will be of interest to see if pristane also incorporates into LDL or other amphipathic structures and is taken up via receptor-mediated endocytosis.[49,73,74] Since pristane is a saturated terpenoid alkane resistant degradation due to the lack of chemically active sidechains, pristane taken up into the lysosomes is likely to be metabolized slowly, if at all. Thus, the gradual accumulation of pristane might promote lysosomal enlargement, LMP, and/or LDCD. Consistent with that possibility, the induction of apoptosis in pristane-exposed Mϕ develops slowly over 48-h or more (Figure 2D).

Autophagy in mice with DAH

Both upregulation and downregulation of autophagy are described in lupus.[75–77] Lipophagy is critically regulated by mTORC1,[78] resulting in the engulfment of lipid droplets by autophagosomes, transfer to lysosomes, and degradation. Assessment of autophagy is complex and the use of multiple assays is recommended.[79] Several lines of evidence suggest that pristane treatment augmented autophagy in myeloid cells. First, the size of autophagic compartments determined by Cyto ID Green staining increased in parallel with neutral lipid (BODIPY and Nile red) staining (Figure 1). This was more prominent in non-classical ($CD138^{+}$) Mϕ and monocytes than in classical ($Ly6C^{hi}$) Mϕ/monocytes. Second, when mice were treated with pristane plus an mTOR inhibitor/

autophagy inducer, BODIPY staining diminished, consistent with lysosomal degradation of neutral lipid (Figure 3A). DAH was exacerbated in mice receiving pristane + rapamycin (Figure 3B). Although the autophagy inhibitor 3MA did not increase BODIPY staining beyond that seen with pristane alone, it substantially reduced the onset of DAH. Using the AO red/green fluorescence ratio as an additional measure of autophagy,[80] both rapamycin and pristane induced a dose-dependent increase autophagy in RAW264.7 Mϕ that was blocked dose-dependently by 3MA (Figure 2B-C). Further, pristane exposure induced the conversion of LC3-I to LC3-II in RAW264.7 cells (Figure 2E).

Since mTOR regulates multiple cell processes,[81] rapamycin could exacerbate DAH by mechanisms other than its effects on autophagy, such as blockade of normal monocyte development.[82,83] Although we cannot formally exclude that possibility, it seems relatively unlikely because 3MA, which blocks autophagy upstream of mTORC1,[84] greatly diminished the severity of DAH and was shown to dose-dependently inhibit the induction of autophagy by rapamycin and pristane in cell culture (Figure 2). Consistent with our results, lipophagy is reduced and foam cell formation is less severe in *ApoE*-/- mice treated with 3MA.[78,85] Notably, foam cell formation in *ApoE*-/- mice is regulated by TremL4[38] and the increased expression of TremL4 protein in monocytes from pristane-treated mice was blocked by NPC1 inhibition (U18666A or cepharanthine) (Figure 4F). Thus, increased TremL4 expression may be involved in the accumulation of lipid-laden monocytes/Mϕ in pristane-treated mice (Figure 1). Along with mTOR, autophagy is critically regulated by Rab7, a small GTPase mediating fusion of autophagosomes with lysosomes.[86] Studies in mice conditionally deficient in *Rab7* or the autophagy protein *Atg7*[87,88] may help to further elucidate the role of autophagy/lipophagy in DAH.

Lysosome dysfunction in DAH

Pristane treatment increased *Plin2* expression, suggestive of lipid overload.[70] Its normalization after rapamycin treatment may indicate that the accumulated lipid droplets were transferred to lysosomes and degraded, as also suggested by the decreased BODIPY staining. Along with increased *Plin2*, lysosome volume enlarged in pristane-treated mice and the expression of *Tfeb* and Tfeb-regulated cathepsin transcripts and protein was higher (Figures 8-9). Increased Lamp-1 staining (Figure 9) also suggested increased lysosomal biogenesis. Autophagy is closely linked to lysosome homeostasis.[78,89,90] When autophagy is excessive, rapid degradation of lysosomal cargo is necessary to prevent lysosomal enlargement, LMP, and LDCD.[15,89,91] It is possible that the increased lysosome volume in pristane-treated mice causes LMP and possibly cytoplasmic leakage of the over-expressed lysosomal cathepsins, which can induce the integrated stress response and cell death.[15,92,93] In

support of this idea, abnormal cathepsin expression is implicated in the pathogenesis in lupus. Renal disease and anti-DNA antibody production are exacerbated in cathepsin S transgenic mice with pristane-induced lupus.[55] Also, cathepsin S protein levels increase in lung, kidney, and other tissues in other murine lupus models and cathepsin S inhibition suppresses lupus nephritis and anti-DNA antibodies,[56,94] possibly by reducing LDCD.[15]

ER stress and DAH are prevented by blocking NPC1

The ER, which normally has a low cholesterol content, is a primary target of cholesterol cytotoxicity.[43] LDCD is blocked by lysosomal cholesterol accumulation.[16,30] Niemann-Pick type C disease is a lysosomal storage disease caused by *NPC1* or *NPC2* mutations.[95] U18666A and cepharanthine, which mimic the Niemann-Pick C disease defect by inhibiting NPC1, potently blocked the onset of pristane-induced DAH (Figure 3C). Niemann-Pick C disease causes progressive neurodegeneration and early death.[95] About 95% of cases are due to *NPC1* mutations and the rest are due to *NPC2* mutations. NPC1 and NPC2 both facilitate the export of free cholesterol from the lysosome into the cytoplasm.[28,96,97] It remains to be determined whether increased *Npc1* and *Npc2* expression in pristane-treated mice (Figure 7J) enhances cytoplasmic free cholesterol transport.

By blocking Npc1, U18666A and cepharanthine trap free cholesterol in the lysosomes, stabilizing the lysosomal membrane and protecting against LMP.[15,16] Both drugs normalized ER stress markers in the lung, but not PECs (Figure 5). It remains to be determined whether these drugs dampen monocyte/Mϕ-mediated lung injury or if they block the effects of cholesterol directly on the lung endothelial cells.[8] Studies in conditional *Npc1* knockout mice will be necessary to resolve this question. Alternatively, NPC1 inhibition might work by down-regulating TremL4 (Figure 4F). The inflammatory response and apoptotic death of myeloid cells are attenuated in *TremL4*-/- mice, which are completely protected from lethal LPS-induced sterile sepsis.[37] TremL4 is expressed mainly by $Ly6C^{lo}$ (non-classical) monocytes.[38] We confirmed the high expression level in that subset (Figure 4F), and found that the $CD138^{+}Ly6C^{-}$ monocyte subset, which is associated with pristane-induced DAH,[4] has the highest expression of all (Figure 4F). Thus, NPC1/2 inhibition may block the pro-apoptotic effects of TremL4 in myeloid cells, though the precise pathways involved remain to be determined.

Clinical implications

Our studies imply a degree of complexity regarding the role of mTOR signaling and autophagy that may not be fully appreciated in lupus. Rapamycin inhibits antigen-induced T cell proliferation and is used to prevent transplant

rejection.[98] It has proven beneficial effects in both murine and human lupus due to the downregulation of proinflammatory T_H1 and T_H17 cells and certain $CD8^+$ T cell subsets.[98] Similarly, metformin inhibits mTOR via AMP-activated protein kinase (AMPK) and has beneficial effects in murine and human lupus.[99,100] However, the mTOR signaling pathway is cell-type dependent.[98] In contrast to its proinflammatory role in T cells, mTOR signaling is anti-inflammatory in Mϕ, favoring M2 over M1 polarization.[101] In transplant patients, rapamycin induces apoptosis of M2 (but not M1) Mϕ and shifts cytokine production toward an M1-like profile [101]. As pristane-induced DAH is a monocyte/Mϕ-driven disorder that can develop in T cell-deficient (*Tcra/Tcrδ* double knockout) mice [102], it is not surprising that despite the reported benefits of rapamycin and metformin in lupus, rapamycin therapy exacerbated DAH in pristane-induced lupus (Figure 3).

Rapamycin (sirolimus), everolimus, metformin, and other mTOR inhibitors are undergoing clinical trials in SLE patients.[103–105] The exacerbation of DAH in pristane-treated mice receiving an mTOR inhibitor is a potential concern because in transplant patients DAH can complicate therapy with rapamycin or the related mTOR inhibitor everolimus.[106–108] The fact that only a small minority of patients treated with these agents develops DAH suggests there is another factor (genetic or environmental) acting synergistically with mTOR inhibition. Similarly, pristane may act synergistically with rapamycin to induce lung injury. Our findings suggest that mTOR inhibitors may need to be used cautiously in SLE.

In summary, we show that pristane-induced lupus alters lipid homeostasis, resulting in autophagy, lysosomal abnormalities, lung inflammation, and myeloid dysregulation. This study suggests that the overall clinical picture in lupus results from the activation of both interferon-dependent (autoantibodies, nephritis) and interferon-independent (DAH) inflammatory pathways.

Materials and Methods

Treatment of mice

Female C57BL/6 (B6) mice (Jackson Laboratory) age 8-12 weeks were maintained under specific pathogen free conditions and injected i.p. with 0.5 ml of pristane (Sigma-Aldrich, #P2870) or mineral oil (MO, C.B. Fleet Co.). Treatment groups consisted of 5-20 mice unless otherwise noted. Experiments were repeated at least twice. Mice in Group 1 treated with U18666A (Selleckchem, #S9669; 10 mg/kg in DMSO every other day from the day of pristane treatment until day 14). U18666A is an amphipathic amine that at nanomolar concentrations selectively blocks cholesterol transport from lysosomes to the ER without a significant effect on transport to the plasma membrane.[39] Group 2 received cepharanthine (Sigma-Aldrich, #SMB00418; 10 mg/kg in DMSO

once daily from the day of pristane treatment until day 14).[31] Cepharanthine is a bisbenzylisoquinoline alkaloid from the tubers of the *Stephania* plant which, like U18666A, selectively blocks cholesterol transport from lysosomes to the ER. Group 3 received the LXR agonist T0901317 (Sigma-Aldrich, #T2320; 10 mg/kg in DMSO once daily from the day of pristane treatment until day 14).[5] Group 4 received avasimibe (Cayman, #18129; 15 mg/kg in DMSO) every other day from the day of pristane treatment until day 14. Avasimibe is an inhibitor of acetyl-CoA acetyltransferase (ACAT1), which esterifies free cholesterol leading to the storage of cholesterol esters in lipid droplets.[18,109] Avasimibe enhances free cholesterol efflux and reduces VLDL cholesterol and total cellular cholesterol content with a variable effect on intracellular free cholesterol.[32,109,110] Group 5 (Control) received pristane and was treated with DMSO-PBS alone. After 14-d, the lungs were assessed for DAH and peripheral blood and peritoneal exudate cells (PECs) were analyzed by flow cytometry.[8] This study followed recommendations of the Animal Welfare Act and US Government Principles for the Utilization and Care of Vertebrate Animals and was approved by the UF IACUC.

Treatment with autophagy activators/inhibitors

B6 mice (7-10 per group) were treated with pristane plus rapamycin (Selleckchem, #S1039; 1.5 mg/kg i.p. every other day) or 3-methyladenine (Selleckchem, S2767; 15 mg/kg i.p. daily), which differentially modulate autophagy and have opposite effects on lipid storage.[25] Rapamycin decreases lipid droplet number and increases lipid droplet-LAMP1 co-localization. It promotes autophagy by blocking mechanistic target of rapamycin complex 1 (mTORC1)-mediated inhibition of autophagy activating kinase. 3-methyladenine inhibits autophagy by blocking class III phosphatidylinositol 3-kinase (PI3K) activity.[84,111] An additional group of 5 mice was treated with pristane + dactolisib (NVP-BEZ235, Selleckchem, S1009; 50 mg/kg/d i.p.). Dactolisib is a dual inhibitor of mTOR and PI3K that binds the ATP-binding cleft of mTOR and PI3K and, like rapamycin, induces autophagy and apoptosis of cancer cells in which the PI3K/Akt/mTOR pathway is constitutively activated.[112,113]

Staining of intracellular and cell surface proteins by flow cytometry

Flow cytometry was performed using anti-mouse CD16/32 (Fc Block, clone 2.4G2, BD Biosciences) before staining with primary antibody or isotype controls. Peritoneal exudate cells (PECs) or peripheral blood (100 µL) was incubated 20-min in the dark with monoclonal antibodies specific for surface markers. After surface-staining, cells were fixed/permeabilized for 5-min (Fix-Perm buffer, #00-5123-43, eBioscience), washed and stained intracellularly for 20-min with anti-CD107a monoclonal antibodies followed by

flow cytometry analysis. Dead cells were gated out using forward and side scatter. Monoclonal antibodies are listed in **Table S1**.

Analysis of neutral lipids and autophagosomes by flow cytometry

Lipid droplets consist of a core of neutral lipids (mainly triacylglycerols and cholesterol esters) surrounded by a phospholipid monolayer and its associated proteins.[114] They are generated from the endoplasmic reticulum (ER) and store neutral lipids, which can be mobilized when needed for metabolism and energy or for membrane and steroid biosynthesis. Lipid droplets can be stained using hydrophobic dyes, such as Nile red and BODIPY 493/503.

Staining with Nile red (9-diethylamino-5H-benzo[alpha]phenoxazine-5-one) (Sigma-Aldrich, #19123) was carried out as described.[115] Nile red detects neutral lipids including triglycerides, cholesterol esters, but not cholesterol or free fatty acids.[116] Cells were co-stained with anti-CD11b, Ly6C, Ly6G, and CD138 antibodies and the mean fluorescence intensity (MFI) of Nile red staining was determined by flow cytometry.

Staining with BODIPY 493/503 (4,4-difluoro-1,3,5,7,8-pentamethyl-4-bora-3a,4a-diaza-*s*-indacene) (ThermoFisher, #D3922), another lipophilic dye that stains neutral lipid in lipid droplets, was carried out as described [117]. Cells were co-stained with anti-CD11b, Ly6C, Ly6G, and CD138 antibodies and the mean fluorescence intensity (MFI) of BODIPY 493/503 was determined by flow cytometry.

The size of autophagic compartments was evaluated by staining with Cyto-ID green (Enzo Life Sciences, CYTO-ID Autophagy Detection Kit) following the manufacturer's protocol. Cyto-ID green dye selectively accumulates in autophagic vacuoles and has been optimized to minimize staining of lysosomes while allowing bright fluorescence when incorporated into pre-autophagosomes.

Evaluation of autophagy by acridine orange staining

Autophagy was measured by analyzing the red to green fluorescence intensity ratio as described.[80] This technique correlates well with western blot analysis of the conversion of unlipidated LC3 into the lipidated form (LC3-I and LC3-II, respectively), SQSTM degradation, and LC3 puncta formation and is more easily quantified.[80]

Western blot analysis of LC3-I to LC3-II conversion

RAW264.7 cells were cultured in DMEM medium containing rapamycin (50 ng/mL) and 10% fetal bovine serum (FBS) or in DMEM containing 5% pristane-saturated FBS and 5% pristane-free FBS in a 2 ml total volume. Cells were

harvested at 24-h, washed, solubilized in sample buffer, and resolved on 12% SDS-polyacrylamide gels. Proteins were transferred to PVDF membranes, and unbound sites were blocked with 5% nonfat dry milk. The blots were probed with monoclonal mouse anti-LC3B antibody (Cell Signaling Technology, Cat # 83506T, 1:1000 dilution) for 12-h followed by rabbit anti mouse secondary antibody (Cell Signaling Technology, 1:1000) for 2 hours. Protein bands were identified by chemiluminescence (Biorad, ChemDoc Touch Imaging System) following the manufacturer's protocols.

Gene expression profiling and quantitative real-time PCR (qPCR)

We analyzed individual transcripts in an RNA-Seq gene expression dataset obtained previously from flow-sorted $CD11b^{+}Ly6C^{hi}CD138^{-}$ and $CD11b^{+}Ly6C^{hi}CD138^{-}$ PECs from pristane and MO treated mice.[118] RNA-Seq data were confirmed by qPCR of total PECs from pristane vs. MO treated mice. qPCR was performed as described[5] using RNA from 10^{6} mouse PEC. Gene expression was normalized to 18S RNA and expression was calculated using the $2^{-\Delta\Delta Ct}$ method. Primer sequences are in Table S2.

LAL enzyme activity

PECs were isolated 14-d after pristane or MO treatment, and LAL enzyme activity was analyzed using the LysoLive™ Lysosomal Acid Lipase Assay kit (Abcam, #ab253380) according to the manufacturer's protocols. Cells were co-stained with anti-CD11b, Ly6C, Ly6G, and CD138 antibodies and the mean fluorescence intensity (MFI) of LAL substrate dye was determined by flow cytometry.

Lysosome volume and pH

PECs were isolated 14-d after pristane or MO treatment and cultured 30 min with LysoTracker DND green (Cell Signaling Technology, #8783; 1:20,000 dilution) or LysoXSensor DND 189 green (ThermoFisher, #L7535; 1:1000 = 1 µM) before analyzing by flow cytometry according to the manufacturer's protocols. The fluorescent probe LysoTracker selectively accumulates in acidic compartments and is a measure of cellular lysosome volume (number and/or size of lysosomes).[119] Autophagic markers and LysoTracker are both upregulated during autophagy.[120] PECs were also stained with anti-CD11b and CD138 antibodies. RAW264.7 cells were grown in DMEM/10% FBS containing pristane/BSA (0-200 µl) as described[4] in the presence or absence of U18666A for 24-h. Cells were analyzed by flow cytometry as above. PECs and RAW 264.7 cells were stained intracellularly with anti-CD107a/lysosomal-associated membrane protein 1 (LAMP-1) antibodies (Biolegend, #W18263B) as a lysosome biogenesis marker.

Cathepsin K activity

Mice were treated with pristane or MO as above and 14-d later, PECs were collected. Enzyme activity of cathepsin K was measured using the Magic Red assay (Immunochemistry Technologies #MR-LR2). The Magic Red reagent is non-fluorescent when taken up into cells and is cleaved by cathepsin K to a cresyl violet fluorophone that is excited at 592 nm and emits at 628 nm. Cresyl violet fluorescence was measured by flow cytometry (BD FACSymphony A3 flow cytometer) in $CD11b^{+}CD138^{+}Ly6G^{-}$ and $CD11b^{+}CD138^{-}Ly6G^{-}$ Mϕ and $CD11b^{+}CD138^{-}Ly6G^{+}$ neutrophils. Cresyl violet generation was measured using the yellow-green laser exciting at 561 nm and measuring emission on the Texas Red channel at 615 nm.

Confocal microscopy

RAW264.7 cells were treated with 10% pristane-saturated FBS, 10% FBS, or chloroquine (30 μM, from Sigma-Aldrich) in DMEM culture medium for 20-h. The cells were washed three times with PBS, LysoTracker Green DND26 (50 nM) and Hoechst 33342 (5 μg/ml, from ThermoFisher) in PBS were added and confocal imaging of live cells was performed immediately using a Leica Stellaris 8 WLL Spectral Confocal Microscope equipped with a variable wavelength White Light Laser (WLL) for fluorescence excitation and a separate 405 nm diode laser for DAPI/Hoechst staining. For BODIPY493/503 and LAMP1 double staining, the treated cells were washed three times with PBS and BODIPY493/503 (600 ng/ml) was added followed by incubation at 37° C for 30-min. Then the cells were fixed with 4% paraformaldehyde and permeabilized with 0.1% Triton X-100. After washing with PBS, the cells were blocked with 2% BSA in PBS for 1-h and incubated with anti-LAMP1-phycoerythrin (1 μg/ml, from BioLegend) and Hoechst 33342 (5 μg/ml) for 1-h. The cells were washed three times with PBS and imaged.

Statistical analysis

Statistical analyses were performed using Prism 6.0 (GraphPad Software). Differences between two sample groups were analyzed by two-sided unpaired Student *t* test unless otherwise. For comparisons involving three or more groups, we used one-way ANOVA. Multiple comparisons were made using Dunnett's multiple comparison test. Data were expressed as mean ± SD. Categorical data were analyzed by χ^2 test. $p < 0.05$ was considered significant.

Acknowledgements

This work was supported by the National Institutes of Health (NIAMS) grant number R01-AR44731 (WR) and by Department of Medicine funding (HZ).

Disclosure Statements

The authors have no potential conflicts of interest.

Funding

This work was supported by the The national insitute of health [R01-AR44731].

ORCID

Shuhong Han http://orcid.org/0000-0002-6951-120X

References

1. Aringer M, Costenbader K, Daikh D, et al. European League Against Rheumatism/American College of Rheumatology Classification Criteria for Systemic Lupus Erythematosus. Arthritis Rheumatol. 2019; 71:1400–12.
2. Reeves WH, Lee PY, Weinstein JS, et al. Induction of autoimmunity by pristane and other naturally occurring hydrocarbons. Trends Immunol. 2009; 30:455–64.
3. Zhuang H, Han S, Lee PY, et al. Pathogenesis of diffuse alveolar hemorrhage in murine lupus. Arthritis Rheumatol. 2017; 69:1280–93 (see commentary).
4. Han S, Zhuang H, Arja RD, et al. A novel monocyte differentiation pattern in pristane-induced lupus with diffuse alveolar hemorrhage. eLife. 2022; 11.
5. Han S, Zhuang H, Shumyak S, et al. Liver X Receptor Agonist Therapy Prevents Diffuse Alveolar Hemorrhage in Murine Lupus by Repolarizing Macrophages. FrontImmunol. 2018; 9:135.
6. Joseph SB, Castrillo A, Laffitte BA, et al. Reciprocal regulation of inflammation and lipid metabolism by liver X receptors. NatMed. 2003; 9:213–9.
7. Tang C, Liu Y, Kessler PS, et al. The macrophage cholesterol exporter ABCA1 functions as an anti-inflammatory receptor. JBiolChem. 2009; 284:32336–43.
8. Zhuang H, Hudson E, Han S, et al. Microvascular lung injury and endoplasmic reticulum stress in SLE-associated alveolar hemorrhage and pulmonary vasculitis. AmJPhysiolLung CellMolPhysiol. 2022; 323:L715–L29.
9. Pineau L, Colas J, Dupont S, et al. Lipid-induced ER stress: synergistic effects of sterols and saturated fatty acids. Traffic. 2009; 10:673–90.
10. Han J, Kaufman RJ. The role of ER stress in lipid metabolism and lipotoxicity. JLipid Res. 2016; 57:1329–38.
11. Frohlich F, Gonzalez Montoro A. The role of lysosomes in lipid homeostasis. BiolChem. 2023; 404:455–65.
12. Chistiakov DA, Melnichenko AA, Myasoedova VA, et al. Mechanisms of foam cell formation in atherosclerosis. JMolMed(Berl). 2017; 95:1153–65.

13. Nagata S. Apoptosis and Clearance of Apoptotic Cells. AnnuRevImmunol. 2018; 36:489–517.
14. Fader Kaiser CM, Romano PS, Vanrell MC, et al. Biogenesis and Breakdown of Lipid Droplets in Pathological Conditions. FrontCell DevBiol. 2021; 9:826248.
15. Wang F, Gomez-Sintes R, Boya P. Lysosomal membrane permeabilization and cell death. Traffic. 2018; 19:918–31.
16. Appelqvist H, Nilsson C, Garner B, et al. Attenuation of the lysosomal death pathway by lysosomal cholesterol accumulation. AmJPathol. 2011; 178:629–39.
17. Han S, Zhuang H, Shumyak S, et al. A novel subset of anti-Inflammatory CD138 (+) macrophages is deficient in mice with experimental lupus. JImmunol. 2017; 199:1261–74.
18. Olzmann JA, Carvalho P. Dynamics and functions of lipid droplets. NatRevMolCell Biol. 2019; 20:137–55.
19. Shiffman D, Mikita T, Tai JT, et al. Large scale gene expression analysis of cholesterol-loaded macrophages. JBiolChem. 2000; 275:37324–32.
20. Larigauderie G, Furman C, Jaye M, et al. Adipophilin enhances lipid accumulation and prevents lipid efflux from THP-1 macrophages: potential role in atherogenesis. ArterioscIerThrombVascBiol. 2004; 24:504–10.
21. Liu XY, Li QS, Yang WH, et al. Inhibition of perilipin 2 attenuates cerebral ischemia/reperfusion injury by blocking NLRP3 inflammasome activation both in vivo and in vitro. In Vitro CellDevBiolAnim. 2023; 59:204–13.
22. McManaman JL, Bales ES, Orlicky DJ, et al. Perilipin-2-null mice are protected against diet-induced obesity, adipose inflammation, and fatty liver disease. JLipid Res. 2013; 54:1346–59.
23. Zhang S, Peng X, Yang S, et al. The regulation, function, and role of lipophagy, a form of selective autophagy, in metabolic disorders. Cell Death Dis. 2022; 13:132.
24. Henne M. And three's a party: lysosomes, lipid droplets, and the ER in lipid trafficking and cell homeostasis. CurrOpinCell Biol. 2019; 59:40–9.
25. Singh R, Kaushik S, Wang Y, et al. Autophagy regulates lipid metabolism. Nature. 2009; 458:1131–5.
26. Loix M, Wouters E, Vanherle S, et al. Perilipin-2 limits remyelination by preventing lipid droplet degradation. CellMolLife Sci. 2022; 79:515.
27. Beesabathuni NS, Park S, Shah PS. Quantitative and temporal measurement of dynamic autophagy rates. Autophagy. 2023; 19:1164–83.
28. Pfeffer SR. NPC intracellular cholesterol transporter 1 (NPC1)-mediated cholesterol export from lysosomes. JBiolChem. 2019; 294:1706–9.
29. Meng Y, Heybrock S, Neculai D, et al. Cholesterol Handling in Lysosomes and Beyond. Trends Cell Biol. 2020; 30:452–66.
30. Appelqvist H, Sandin L, Bjornstrom K, et al. Sensitivity to lysosome-dependent cell death is directly regulated by lysosomal cholesterol content. PloS one. 2012; 7:e50262.
31. Lyu J, Yang EJ, Head SA, et al. Pharmacological blockade of cholesterol trafficking by cepharanthine in endothelial cells suppresses angiogenesis and tumor growth. Cancer Lett. 2017; 409:91–103.
32. Zabielska J, Sledzinski T, Stelmanska E. Acyl-Coenzyme A: Cholesterol Acyltransferase Inhibition in Cancer Treatment. Anticancer Res. 2019; 39:3385–94.
33. Cyster JG, Dang EV, Reboldi A, et al. 25-Hydroxycholesterols in innate and adaptive immunity. NatRevImmunol. 2014; 14:731–43.

34. Blanc M, Hsieh WY, Robertson KA, et al. The transcription factor STAT-1 couples macrophage synthesis of 25-hydroxycholesterol to the interferon antiviral response. Immunity. 2013; 38:106–18.
35. Spann NJ, Glass CK. Sterols and oxysterols in immune cell function. NatImmunol. 2013; 14:893–900.
36. Madenspacher JH, Morrell ED, McDonald JG, et al. 25-hydroxycholesterol exacerbates vascular leak during acute lung injury. JCI Insight. 2023.
37. Nedeva C, Menassa J, Duan M, et al. TREML4 receptor regulates inflammation and innate immune cell death during polymicrobial sepsis. NatImmunol. 2020; 21:1585–96.
38. Gonzalez-Cotto M, Guo L, Karwan M, et al. TREML4 Promotes Inflammatory Programs in Human and Murine Macrophages and Alters Atherosclerosis Lesion Composition in the Apolipoprotein E Deficient Mouse. FrontImmunol. 2020; 11:397.
39. Lu F, Liang Q, Abi-Mosleh L, et al. Identification of NPC1 as the target of U18666A, an inhibitor of lysosomal cholesterol export and Ebola infection. eLife 2015; 4.
40. Tabas I. Consequences of cellular cholesterol accumulation: basic concepts and physiological implications. JClinInvest. 2002; 110:905–11.
41. Halbleib K, Pesek K, Covino R, et al. Activation of the Unfolded Protein Response by Lipid Bilayer Stress. MolCell. 2017; 67:673–84 e8.
42. Watkin LB, Jessen B, Wiszniewski W, et al. COPA mutations impair ER-Golgi transport and cause hereditary autoimmune-mediated lung disease and arthritis. NatGenet. 2015; 47:654–60.
43. Feng B, Yao PM, Li Y, et al. The endoplasmic reticulum is the site of cholesterol-induced cytotoxicity in macrophages. NatCell Biol. 2003; 5:781–92.
44. Hu H, Tian M, Ding C, Yu S. The C/EBP Homologous Protein (CHOP) Transcription Factor Functions in Endoplasmic Reticulum Stress-Induced Apoptosis and Microbial Infection. FrontImmunol. 2018; 9:3083.
45. Dubland JA, Francis GA. Lysosomal acid lipase: at the crossroads of normal and atherogenic cholesterol metabolism. FrontCell DevBiol. 2015; 3:3.
46. Samstad EO, Niyonzima N, Nymo S, et al. Cholesterol crystals induce complement-dependent inflammasome activation and cytokine release. JImmunol. 2014; 192:2837–45.
47. Li H, Cao Z, Wang L, et al. Macrophage Subsets and Death Are Responsible for Atherosclerotic Plaque Formation. FrontImmunol. 2022; 13:843712.
48. Korbelius M, Kuentzel KB, Bradic I, et al. Recent insights into lysosomal acid lipase deficiency. Trends MolMed. 2023; 29:425–38.
49. Chistiakov DA, Bobryshev YV, Orekhov AN. Macrophage-mediated cholesterol handling in atherosclerosis. JCellMolMed. 2016; 20:17–28.
50. Lian X, Yan C, Yang L, et al. Lysosomal acid lipase deficiency causes respiratory inflammation and destruction in the lung. AmJPhysiolLung CellMolPhysiol. 2004; 286:L801–7.
51. Scarcella M, d'Angelo D, Ciampa M, et al. The Key Role of Lysosomal Protease Cathepsins in Viral Infections. IntJMolSci. 2022; 23.
52. Roberg K, Kagedal K, Ollinger K. Microinjection of cathepsin d induces caspase-dependent apoptosis in fibroblasts. AmJPathol. 2002; 161:89–96.
53. Deiss LP, Galinka H, Berissi H, et al. Cathepsin D protease mediates programmed cell death induced by interferon-gamma, Fas/APO-1 and TNF-alpha. EMBO J. 1996; 15:3861–70.

54. Steffensen KR, Jakobsson T, Gustafsson JA. Targeting liver X receptors in inflammation. Expert opinion on therapeutic targets. 2013; 17:977–90.
55. Lee J, Jang S, Choi M, et al. Overexpression of cathepsin S exacerbates lupus pathogenesis through upregulation TLR7 and IFN-alpha in transgenic mice. SciRep. 2021; 11:16348.
56. Yen TH, Ho WJ, Yeh YH, et al. Cathepsin S Inhibition Suppresses Experimental Systemic Lupus Erythematosus-Associated Pulmonary Arterial Remodeling. IntJMolSci. 2022; 23.
57. Phi NC, Chien DK, Binh VV, et al. Cathepsin D-like activity in serum of patients with systemic lupus erythematosus. JClinLabImmunol. 1989; 29:185–8.
58. Zhou Y, Chen H, Liu L, et al. Cathepsin K Deficiency Ameliorates Systemic Lupus Erythematosus-like Manifestations in Fas(lpr) Mice. JImmunol. 2017; 198:1846–54.
59. Saftig P, Puertollano R. How Lysosomes Sense, Integrate, and Cope with Stress. Trends BiochemSci. 2021; 46:97–112.
60. Barral DC, Staiano L, Guimas Almeida C, et al. Current methods to analyze lysosome morphology, positioning, motility and function. Traffic. 2022; 23:238–69.
61. Settembre C, Fraldi A, Medina DL, et al. Signals from the lysosome: a control centre for cellular clearance and energy metabolism. NatRevMolCell Biol. 2013; 14:283–96.
62. Lu S, Sung T, Lin N, et al. Lysosomal adaptation: How cells respond to lysosomotropic compounds. PloS one. 2017; 12:e0173771.
63. Logan R, Kong AC, Axcell E, et al. Amine-containing molecules and the induction of an expanded lysosomal volume phenotype: a structure-activity relationship study. JPharmSci. 2014; 103:1572–80.
64. Anderson N, Borlak J. Drug-induced phospholipidosis. FEBS letters. 2006; 580:5533–40.
65. Gawrisch K, Janz S. The uptake of pristane (2,6,10,14-tetramethylpentadecane) into phospholipid bilayers as assessed by NMR, DSC, and tritium labeling methods. BiochimBiophysActa. 1991; 1070:409–18.
66. Scerra G, Caporaso MG, Renna M, D'Agostino M. Protocol for labeling and fixation of intact lysosomes with esterified amino acid analogs to assess lysosomal expansion in living eukaryotic cells. STAR Protoc 2021; 2:100916.
67. Xu Y, Du X, Turner N, et al. Enhanced acyl-CoA:cholesterol acyltransferase activity increases cholesterol levels on the lipid droplet surface and impairs adipocyte function. JBiolChem. 2019; 294:19306–21.
68. Zechner R, Madeo F, Kratky D. Cytosolic lipolysis and lipophagy: two sides of the same coin. NatRevMolCell Biol. 2017; 18:671–84.
69. Beller M, Sztalryd C, Southall N, et al. COPI complex is a regulator of lipid homeostasis. PLoS Biol. 2008; 6:e292.
70. Buechler C, Ritter M, Duong CQ, et al. Adipophilin is a sensitive marker for lipid loading in human blood monocytes. BiochimBiophysActa. 2001; 1532:97–104.
71. Satoh M, Kuroda Y, Yoshida H, et al. Induction of lupus autoantibodies by adjuvants. JAutoimm. 2003; 21:1–9.
72. Simonen PP, Gylling H, Miettinen TA. The distribution of squalene and noncholesterol sterols in lipoproteins in type 2 diabetes. Atherosclerosis. 2007; 194:222–9.
73. Gianturco SH, Lin AH, Hwang SL, et al. Distinct murine macrophage receptor pathway for human triglyceride-rich lipoproteins. JClinInvest. 1988; 82:1633–43.

74. Febbraio M, Podrez EA, Smith JD, et al. Targeted disruption of the class B scavenger receptor CD36 protects against atherosclerotic lesion development in mice. JClinInvest. 2000; 105:1049–56.
75. Li B, Yue Y, Dong C, et al. Blockade of macrophage autophagy ameliorates activated lymphocytes-derived DNA induced murine lupus possibly via inhibition of proinflammatory cytokine production. ClinExpRheumatol. 2014; 32:705–14.
76. Hsu HC, Chen YH, Lin TS, et al. Systemic lupus erythematosus is associated with impaired autophagic degradation via interleukin-6 in macrophages. BiochimBiophysActa MolBasis Dis. 2021; 1867:166027.
77. Jang A, Sharp R, Wang JM, et al. Dependence on Autophagy for Autoreactive Memory B Cells in the Development of Pristane-Induced Lupus. FrontImmunol. 2021; 12:701066.
78. Tegeder I, Kogel D. When lipid homeostasis runs havoc: Lipotoxicity links lysosomal dysfunction to autophagy. Matrix Biol. 2021; 100-101:99–117.
79. Klionsky DJ, Abdelmohsen K, Abe A, et al. Guidelines for the use and interpretation of assays for monitoring autophagy. (3rd edition). Autophagy 2016; 12:1–222.
80. Thome MP, Filippi-Chiela EC, Villodre ES, et al. Ratiometric analysis of Acridine Orange staining in the study of acidic organelles and autophagy. JCell Sci. 2016; 129:4622–32.
81. Laplante M, Sabatini DM. mTOR signaling in growth control and disease. Cell. 2012; 149:274–93.
82. Lee PY, Sykes DB, Ameri S, et al. The metabolic regulator mTORC1 controls terminal myeloid differentiation. SciImmunol. 2017; 2:eaam6641.
83. Lee PY, Nelson-Maney N, Huang Y, et al. High-dimensional analysis reveals a pathogenic role of inflammatory monocytes in experimental diffuse alveolar hemorrhage. JCI Insight. 2019; 4.
84. Wu YT, Tan HL, Shui G, et al. Dual role of 3-methyladenine in modulation of autophagy via different temporal patterns of inhibition on class I and III phosphoinositide 3-kinase. JBiolChem. 2010; 285:10850–61.
85. Dai S, Wang B, Li W, et al. Systemic application of 3-methyladenine markedly inhibited atherosclerotic lesion in ApoE(-/-) mice by modulating autophagy, foam cell formation and immune-negative molecules. Cell Death Dis. 2016; 7: e2498.
86. Baba T, Toth DJ, Sengupta N, et al. Phosphatidylinositol 4,5-bisphosphate controls Rab7 and PLEKHM1 membrane cycling during autophagosome-lysosome fusion. The EMBO journal. 2019; 38:e100312.
87. Schroeder B, Schulze RJ, Weller SG, et al. The small GTPase Rab7 as a central regulator of hepatocellular lipophagy. Hepatology. 2015; 61:1896–907.
88. Camprecios G, Anton A, Oncins A, et al. Lack of endothelial autophagy does not impair liver regeneration after partial hepatectomy in mice. Liver Int. 2023.
89. Patra S, Patil S, Klionsky DJ, et al. Lysosome signaling in cell survival and programmed cell death for cellular homeostasis. JCellPhysiol. 2023; 238:287–305.
90. Settembre C, Di Malta C, Polito VA, et al. TFEB links autophagy to lysosomal biogenesis. Science. 2011; 332:1429–33.
91. Ono K, Kim SO, Han J. Susceptibility of lysosomes to rupture is a determinant for plasma membrane disruption in tumor necrosis factor alpha-induced cell death. MolCellBiol. 2003; 23:665–76.
92. Tian AL, Wu Q, Liu P, et al. Lysosomotropic agents including azithromycin, chloroquine and hydroxychloroquine activate the integrated stress response. Cell Death Dis. 2021; 12:6.

93. Boya P, Kroemer G. Lysosomal membrane permeabilization in cell death. Oncogene. 2008; 27:6434–51.
94. Rupanagudi KV, Kulkarni OP, Lichtnekert J, et al. Cathepsin S inhibition suppresses systemic lupus erythematosus and lupus nephritis because cathepsin S is essential for MHC class II-mediated CD4 T cell and B cell priming. AnnRheumDis. 2015; 74:452–63.
95. Platt N, Speak AO, Colaco A, et al. Immune dysfunction in Niemann-Pick disease type C. JNeurochem. 2016; 136 Suppl 1:74–80.
96. Yu XH, Jiang N, Yao PB, et al. NPC1, intracellular cholesterol trafficking and atherosclerosis. ClinChimActa. 2014; 429:69–75.
97. Chang TY, Chang CC, Ohgami N, et al. Cholesterol sensing, trafficking, and esterification. AnnuRevCell DevBiol. 2006; 22:129–57.
98. Perl A. Activation of mTOR (mechanistic target of rapamycin) in rheumatic diseases. NatRevRheumatol. 2016; 12:169–82.
99. Yin Y, Choi SC, Xu Z, et al. Normalization of CD4+ T cell metabolism reverses lupus. SciTranslMed. 2015; 7:274ra18.
100. Sun F, Geng S, Wang H, et al. Effects of metformin on disease flares in patients with systemic lupus erythematosus: post hoc analyses from two randomised trials. Lupus SciMed. 2020; 7.
101. Mercalli A, Calavita I, Dugnani E, et al. Rapamycin unbalances the polarization of human macrophages to M1. Immunology. 2013; 140:179–90.
102. Barker TT, Lee PY, Kelly-Scumpia KM, et al. Pathogenic role of B cells in the development of diffuse alveolar hemorrhage induced by pristane. LabInvest. 2011; 91:1540–50.
103. Zhang L, Cui JY, Zhang L. Clinical efficacy and safety of sirolimus in childhood-onset systemic lupus erythematosus in real world. Medicine (Baltimore). 2022; 101:e31551.
104. Jiang N, Li M, Zhang H, et al. Sirolimus versus tacrolimus for systemic lupus erythematosus treatment: results from a real-world CSTAR cohort study. Lupus SciMed. 2022; 9.
105. Okita Y, Yoshimura M, Katada Y, et al. A mechanistic target of rapamycin inhibitor, everolimus safely ameliorated lupus nephritis in a patient complicated with tuberous sclerosis. ModRheumatolCase Rep. 2023; 7:47–51.
106. Balcan B, Simsek E, Ugurlu AO, et al. Sirolimus-Induced Diffuse Alveolar Hemorrhage: A Case Report. AmJTher. 2016; 23:e1938–e41.
107. Vlahakis NE, Rickman OB, Morgenthaler T. Sirolimus-associated diffuse alveolar hemorrhage. Mayo ClinProc. 2004; 79:541–5.
108. Vandewiele B, Vandecasteele SJ, Vanwalleghem L, et al. Diffuse alveolar hemorrhage induced by everolimus. Chest. 2010; 137:456–9.
109. Llaverias G, Laguna JC, Alegret M. Pharmacology of the ACAT inhibitor avasimibe (CI-1011). CardiovascDrug Rev. 2003; 21:33–50.
110. Zhu Y, Chen CY, Li J, et al. In vitro exploration of ACAT contributions to lipid droplet formation during adipogenesis. JLipid Res. 2018; 59:820–9.
111. Seglen PO, Gordon PB. 3-Methyladenine: specific inhibitor of autophagic/lysosomal protein degradation in isolated rat hepatocytes. ProcNatlAcadSciUSA. 1982; 79:1889–92.
112. Maira SM, Stauffer F, Brueggen J, et al. Identification and characterization of NVP-BEZ235, a new orally available dual phosphatidylinositol 3-kinase/mammalian target of rapamycin inhibitor with potent in vivo antitumor activity. MolCancer Ther. 2008; 7:1851–63.

113. Ma Y, Jin Z, Yu K, et al. NVP-BEZ235-induced autophagy as a potential therapeutic approach for multiple myeloma. AmJTranslRes. 2019; 11:87–105.
114. Martin S, Parton RG. Lipid droplets: a unified view of a dynamic organelle. NatRevMolCell Biol. 2006; 7:373–8.
115. Greenspan P, Mayer EP, Fowler SD. Nile red: a selective fluorescent stain for intracellular lipid droplets. JCell Biol. 1985; 100:965–73.
116. Boumelhem BB, Pilgrim C, Zwicker VE, et al. Intracellular flow cytometric lipid analysis - a multiparametric system to assess distinct lipid classes in live cells. JCellSci. 2022; 135.
117. Qiu B, Simon MC. BODIPY 493/503 Staining of Neutral Lipid Droplets for Microscopy and Quantification by Flow Cytometry. Bio Protoc. 2016; 6.
118. Han S, Zhuang H, Lee PY, et al. Differential Responsiveness of Monocyte and Macrophage Subsets to Interferon. Arthritis Rheumatol. 2020; 72:100–13.
119. te Vruchte D, Speak AO, Wallom KL, et al. Relative acidic compartment volume as a lysosomal storage disorder-associated biomarker. JClinInvest. 2014; 124:1320–8.
120. Chikte S, Panchal N, Warnes G. Use of LysoTracker dyes: a flow cytometric study of autophagy. Cytometry A. 2014; 85:169–78.